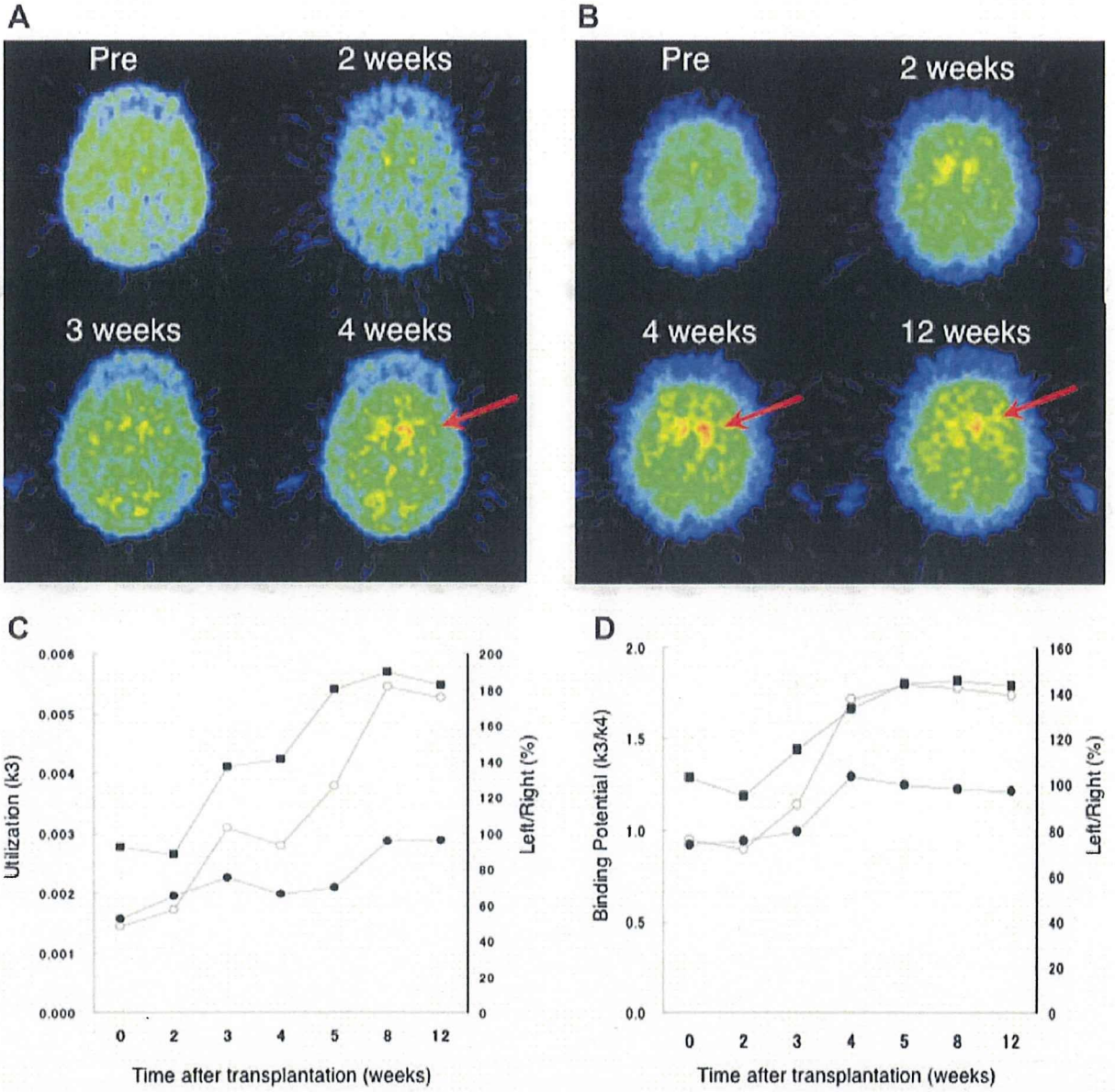

Fig. 2. (A, B) PET images of L-[β-^{11}C]DOPA (A) and [^{11}C]β-CFT (B) uptake in monkey M-1 before and after cell transplantation. Four weeks after implantation, increased radionuclide uptake was detected in the implanted putamen (arrows). (C, D) Graphic representation of relative changes in signal strength over time in the same animal, showing significant increases in L-[β-^{11}C]DOPA utilization (k_3 value) (C) and [^{11}C]β-CFT binding potential (BP) (k_3/k_4 value) (D) in the implanted (left: open circles) putamen compared with control (right: filled circles) putamen. Filled squares indicate left to right ratio.

respectively. Many TH-IR cells, about 1000 in M-1 and 3000 in M-2, thrived in the grafted putamen (Fig. 4). Less than 50 TH-IR cells were found in the putamen on the side contralateral to the graft. A small number of 5HT-IR cells was identified in the grafted putamen (<5 cells). No TH-positive cells were positive for the proliferation marker Ki-67. Hematoxylin and eosin staining showed no signs of teratoma-like structures in the transplanted putamen.

DISCUSSION

This study demonstrated with PET that engraftment of NSCs derived from primate ES cells has the capacity to restore DA function in a primate model of PD. Transplantation of neural precursors has become one of the key strategies for cell replacement in the brain. To bypass the shortage of donor tissue, a wide range of experimental approaches have been studied, including proliferation of NSCs in vitro stimulated by

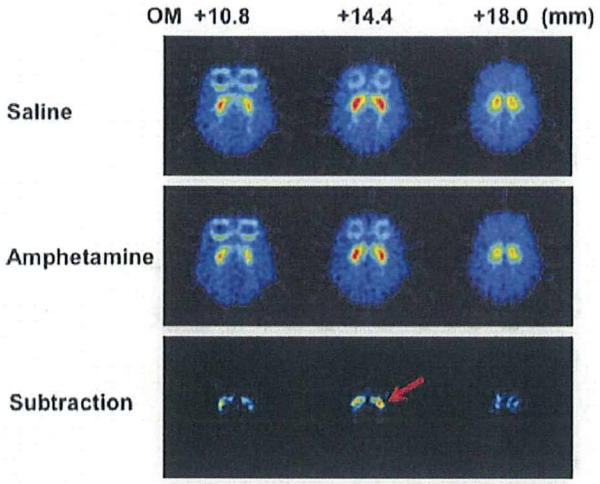

Fig. 3. Drug-induced release of DA in the grafted striatum 12 weeks after transplantation in monkey M-2. After methamphetamine administration, [^{11}C]raclopride binding in the implanted putamen was significantly reduced compared with that in the control putamen. Each slice image after methamphetamine infusion (middle row) was subtracted from a corresponding baseline image (upper row). Subtraction images (lower row). The images of each column are in horizontal plane and same stereotaxic coordinates (mm) from the orbitomeatal (OM) line. Arrows indicate the side of the implant.

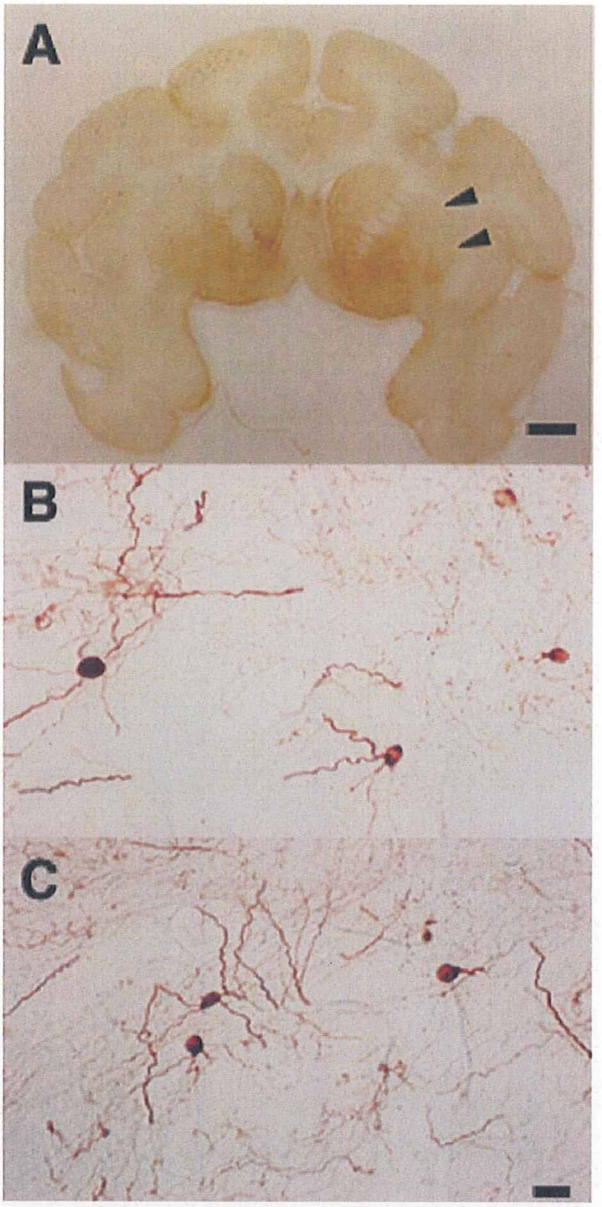

Fig. 4. TH-IR cells in the unilateral putamen of monkey M-1 at 3 months after cell implantation. (**A**) Restoration of TH-IR in the implanted putamen (arrowhead) is not obvious at low magnification. However, TH-IR neurons are apparent in dorsal (**B**) and ventral (**C**) portions of the implanted putamen. Scale bar: 0.5 cm (A); 20 μm (B, C).

mitogen treatment, ex vivo introduction of growth stimulating oncogenes, xenotransplantation, enhancement of endogenous adult neurogenesis, and attempts to recruit non-neural adult stem cells from other tissues (Hall et al., 2007; Liu, 2008). However, in addition to the limited plasticity and slow propagation of adult stem cells, continuous expression of oncogenes or stimulation of mitogens raises question about the long-term safety of these strategies. Of the various candidate donor cells, ES cells are the most attractive due to the characteristics of pluripotency and the potential for unlimited self-renewal. Although human ES cells seem promising for clinical applications, an alternative model system based on ES cells derived from nonhuman primates is necessary for preclinical studies, including allogenic transplantation.

The present study used cynomolgus monkey ES cells that resemble human ES cells but are distinct from murine ES cells in terms of morphology, expression of surface markers and feeder- and leukemia inhibitory factor-dependence, among other factors (Suemori et al., 2001). We have previously shown that astrocyte-derived factors instruct mouse and primate ES cells to differentiate into neurons quickly and efficiently (Nakayama et al., 2003, 2004). This ACM method is superior to previous methods in terms of simplicity, efficiency, and productivity of neural differentiation. The number of cells was increased 1000-fold, along with differentiation from ES cells into NSCs. NSCs can be highly purified without using either magnetic- or fluorescence-activated cell sorting, and incorporation of undifferentiated ES cells is virtually eliminated. Although low doses of undifferentiated mouse ES cells transplanted into rat striatum developed into fully differentiated DA neurons (Bjorklund et al., 2002), elimination of undifferentiated ES cells is crucial for reducing the risk of tumor formation. Consistent with our previous observations,

culture of NSCs derived from cynomolgus monkey ES cells on an adhesive substrate in ACM exclusively promoted differentiation into neurons.

Parkinsonian features were induced by intravenous administration of MPTP over a period of several months. MPTP causes slowly progressive loss of DA neurons in the substantia nigra, resulting in primates showing all the clinical signs of PD, including tremor, rigidity, akinesia, and postural instability (Wichmann and DeLong, 2003). We created bilateral striatal lesions but implanted cells unilaterally, so one side could serve as a control. Functional effects of the graft were evaluated by comparing PET images of the implanted putamen with those of the contralateral putamen. PET can be used to assess DA function in vivo (Brooks, 2004) by following increases in L-[β-^{11}C]DOPA uptake or [^{11}C]β-CFT binding, which are attributable to the expression of AADC and storage of DA in the putamen and thus indicate graft survival and development of DA neurons. In addition, functional DA release from the graft was demonstrated by imaging D_2 receptor occupancy. Degrees of decrease in striatal radioactivity of [^{11}C]raclopride after amphetamine challenge were significantly higher in the grafted putamen. Based on microdialysis studies, a 1% change in striatal [^{11}C]raclopride binding has been estimated to correspond to a $\geq$8% change in synaptic DA levels (Breier et al., 1997). We identified numerous TH neurons in the grafted putamen. Although small populations of TH neurons may be found in the primate striatum after creating lesions of the nigrostriatal dopaminergic pathways, most are located in the caudate and precommissural putamen (Mazloom and Smith, 2006). The dramatic increase in the number of TH-IR cells in the postcommissural putamen suggests that these TH-IR cells were derived from the graft and contributed to the restoration of dopaminergic function.

Behavioral recovery was modest at 12 weeks after implantation. More DA neurons and synaptic DA release might be necessary for apparent behavioral recovery. Improving neuronal survival and increasing axonal outgrowth would possibly improve the magnitude of the response to grafting. In this regard, the combination of cell replacement and neuroprotective strategies by gene delivery may be effective in preventing the loss of endogenous and grafted NSCs. Another possible explanation for incomplete behavioral recovery is that functional integration of DA neurons with the host circuitry may take place gradually. PD patients with implanted fetal DA neurons show continuous symptomatic improvements even after DA storage capacity in the striatum (measured by L-[β-^{11}C]DOPA PET) and response to DA-releasing agents has plateaued (Isacson et al., 2001; Piccini et al., 2000). With bilateral implantation, further amelioration of global parkinsonism (including enhanced spontaneous activity and improved balance) would be expected, since only 20% of thalamic projections from the basal ganglia are crossed in monkeys (Parent and Hazrati, 1995) and unilateral implantation would mainly affect contralateral limb movement. Monkeys did not display dyskinesia with or without L-dopa. This result supports previous observations that functional DA grafts do not independently generate abnormal DA responses (Bjorklund et al., 2002).

Given the recent successful isolation of nuclear-transferred ES cell lines (Tabar et al., 2008), our findings of efficient ES cell transplantation, expansion, and differentiation into functional DA neurons in the primate model have implications for ES cells as a donor source for cell therapy against PD.

ACKNOWLEDGMENTS

The authors thank Astellas Pharmaceuticals (Osaka, Japan) for providing FK506.

REFERENCES

Bjorklund LM, Sanchez-Pernaute R, Chung S, Andersson T, Chen IY, McNaught KS, Brownell AL, Jenkins BG, Wahlestedt C, Kim KS, Isacson O. 2002. Embryonic stem cells develop into functional dopaminergic neurons after transplantation in a Parkinson rat model. Proc Natl Acad Sci USA 99:2344–2349.

Breier A, Su TP, Saunders R, Carson RE, Kolachana BS, de Bartolomeis A, Weinberger DR, Weisenfeld N, Malhotra AK, Eckelman WC, Pickar D. 1997. Schizophrenia is associated with elevated amphetamine-induced synaptic dopamine concentrations: Evidence from a novel positron emission tomography method. Proc Natl Acad Sci USA 94:2569–2574.

Brooks DJ. 2004. Positron emission tomography imaging of transplant function. NeuroRx 1:482–491.

Chung S, Shin BS, Hwang M, Lardaro T, Kang UJ, Isacson O, Kim KS. 2006. Neural precursors derived from embryonic stem cells, but not those from fetal ventral mesencephalon, maintain the potential to differentiate into dopaminergic neurons after expansion in vitro. Stem Cells 24:1583–1593.

Hall VJ, Li JY, Brundin P. 2007. Restorative cell therapy for Parkinson's disease: A quest for the perfect cell. Semin Cell Dev Biol 18:859–869.

Huang SC, Barrio JR, Phelps ME. 1986. Neuroreceptor assay with positron emission tomography: Equilibrium versus dynamic approaches. J Cereb Blood Flow Metab 6:515–521.

Inoue N, Matsui H, Tsukui H, Hatanaka H. 1988. The appearance of a highly digitalis-sensitive isoform of Na+,K+-ATPase during maturation in vitro of primary cultured rat cerebral neurons. J Biochem (Tokyo) 104:349–354.

Isacson O, Bjorklund L, Pernaute RS. 2001. Parkinson's disease: Interpretations of transplantation study are erroneous. Nat Neurosci 4:553.

Jenner P. 2000. Factors influencing the onset and persistence of dyskinesia in MPTP-treated primates. Ann Neurol 47 (4 Suppl 1): S90–S99; discussion S99–S104.

Kim JH, Auerbach JM, Rodriguez-Gomez JA, Velasco I, Gavin D, Lumelsky N, Lee SH, Nguyen J, Sanchez-Pernaute R, Bankiewicz K, McKay R. 2002. Dopamine neurons derived from embryonic stem cells function in an animal model of Parkinson's disease. Nature 418:50–56.

Kish SJ, Shannak K, Hornykiewicz O. 1988. Uneven pattern of dopamine loss in the striatum of patients with idiopathic Parkinson's disease. Pathophysiologic and clinical implications. N Engl J Med 318:876–880.

Li JY, Christophersen NS, Hall V, Soulet D, Brundin P. 2008. Critical issues of clinical human embryonic stem cell therapy for brain repair. Trends Neurosci 31:146–153.

Liu SV. 2008. iPS cells: A more critical review. Stem Cells Dev 17:391–397.

Mazloom M, Smith Y. 2006. Synaptic microcircuitry of tyrosine hydroxylase-containing neurons and terminals in the striatum

of 1-methyl-4-phenyl-1,2,3,6-tetrahydropyridine-treated monkeys. J Comp Neurol 495:453–469.
Nakayama T, Momoki-Soga T, Inoue N. 2003. Astrocyte-derived factors instruct differentiation of embryonic stem cells into neurons. Neurosci Res 46:241–249.
Nakayama T, Momoki-Soga T, Yamaguchi K, Inoue N. 2004. Efficient production of neural stem cells and neurons from embryonic stem cells. Neuroreport 15:487–491.
Newman MB, Bakay RA. 2008. Therapeutic potentials of human embryonic stem cells in Parkinson's disease. Neurotherapeutics 5:237–251.
Parent A, Hazrati LN. 1995. Functional anatomy of the basal ganglia. I. The cortico-basal ganglia-thalamo-cortical loop. Brain Res Brain Res Rev 20:91–127.
Piccini P, Lindvall O, Bjorklund A, Brundin P, Hagell P, Ceravolo R, Oertel W, Quinn N, Samuel M, Rehncrona S, Widner H, Brooks DJ. 2000. Delayed recovery of movement-related cortical function in Parkinson's disease after striatal dopaminergic grafts. Ann Neurol 48:689–695.
Rodriguez-Gomez JA, Lu JQ, Velasco I, Rivera S, Zoghbi SS, Liow JS, Musachio JL, Chin FT, Toyama H, Seidel J, Green MV, Thanos PK, Ichise M, Pike VW, Innis RB, McKay RD. 2007. Persistent dopamine functions of neurons derived from embryonic stem cells in a rodent model of Parkinson disease. Stem Cells 25:918–928.
Sanchez-Pernaute R, Studer L, Ferrari D, Perrier A, Lee H, Vinuela A, Isacson O. 2005. Long-term survival of dopamine neurons derived from parthenogenetic primate embryonic stem cells (cyno-1) after transplantation. Stem Cells 23:914–922.
Suemori H, Tada T, Torii R, Hosoi Y, Kobayashi K, Imahie H, Kondo Y, Iritani A, Nakatsuji N. 2001. Establishment of embryonic stem cell lines from cynomolgus monkey blastocysts produced by IVF or ICSI. Dev Dyn 222:273–279.
Tabar V, Tomishima M, Panagiotakos G, Wakayama S, Menon J, Chan B, Mizutani E, Al-Shamy G, Ohta H, Wakayama T, Studer L. 2008. Therapeutic cloning in individual parkinsonian mice. Nat Med 14:379–381.
Takagi Y, Takahashi J, Saiki H, Morizane A, Hayashi T, Kishi Y, Fukuda H, Okamoto Y, Koyanagi M, Ideguchi M, Hayashi H, Imazato T, Kawasaki H, Suemori H, Omachi S, Iida H, Itoh N, Nakatsuji N, Sasai Y, Hashimoto N. 2005. Dopaminergic neurons generated from monkey embryonic stem cells function in a Parkinson primate model. J Clin Invest 115:102–109.
Tsukada H, Harada N, Nishiyama S, Ohba H, Kakiuchi T. 2000a. Cholinergic neuronal modulation alters dopamine D2 receptor availability in vivo by regulating receptor affinity induced by facilitated synaptic dopamine turnover: Positron emission tomography studies with microdialysis in the conscious monkey brain. J Neurosci 20:7067–7073.
Tsukada H, Harada N, Nishiyama S, Ohba H, Sato K, Fukumoto D, Kakiuchi T. 2000b. Ketamine decreased striatal [(11)C]raclopride binding with no alterations in static dopamine concentrations in the striatal extracellular fluid in the monkey brain: Multiparametric PET studies combined with microdialysis analysis. Synapse 37:95–103.
Watanabe M, Okada H, Shimizu K, Omura T, Yoshikawa E, Kosugi T, Mori S, Yamashita T. 1997. A high resolution animal PET scanner using compact PS-PMT detectors. IEEE Trans Nucl Sci 44:1277–1282.
Wichmann T, DeLong MR. 2003. Pathophysiology of Parkinson's disease: The MPTP primate model of the human disorder. Ann N Y Acad Sci 991:199–213.

OPEN ACCESS Freely available online

PLoS one

Self-Contained Induction of Neurons from Human Embryonic Stem Cells

Tsuyoshi Okuno[1,2], Takashi Nakayama[3], Nae Konishi[1], Hideo Michibata[1], Koji Wakimoto[1], Yutaka Suzuki[1], Shinji Nito[1], Toshio Inaba[2], Imaharu Nakano[4], Shin-ichi Muramatsu[4], Makoto Takano[5], Yasushi Kondo[1]*, Nobuo Inoue[6]

1 Advanced Medical Research Laboratory, Mitsubishi Tanabe Pharma Corporation, Osaka, Japan, **2** Department of Advanced Pathobiology, Graduate School of Life and Environmental Sciences, Osaka Prefecture University, Osaka, Japan, **3** Department of Biochemistry, Yokohama City University School of Medicine, Yokohama, Japan, **4** Division of Neurology, Department of Medicine, Jichi Medical University, Tochigi, Japan, **5** Department of Physiology, Jichi Medical University, Tochigi, Japan, **6** Laboratory of Regenerative Neurosciences, Graduate School of Human Health Sciences, Tokyo Metropolitan University, Tokyo, Japan

Abstract

Background: Neurons and glial cells can be efficiently induced from mouse embryonic stem (ES) cells in a conditioned medium collected from rat primary-cultured astrocytes (P-ACM). However, the use of rodent primary cells for clinical applications may be hampered by limited supply and risk of contamination with xeno-proteins.

Methodology/Principal Findings: We have developed an alternative method for unimpeded production of human neurons under xeno-free conditions. Initially, neural stem cells in sphere-like clusters were induced from human ES (hES) cells after being cultured in P-ACM under free-floating conditions. The resultant neural stem cells could circumferentially proliferate under subsequent adhesive culture, and selectively differentiate into neurons or astrocytes by changing the medium to P-ACM or G5, respectively. These hES cell-derived neurons and astrocytes could procure functions similar to those of primary cells. Interestingly, a conditioned medium obtained from the hES cell-derived astrocytes (ES-ACM) could successfully be used to substitute P-ACM for induction of neurons. Neurons made by this method could survive in mice brain after xeno-transplantation.

Conclusion/Significance: By inducing astrocytes from hES cells in a chemically defined medium, we could produce human neurons without the use of P-ACM. This self-serving method provides an unlimited source of human neural cells and may facilitate clinical applications of hES cells for neurological diseases.

Citation: Okuno T, Nakayama T, Konishi N, Michibata H, Wakimoto K, et al. (2009) Self-Contained Induction of Neurons from Human Embryonic Stem Cells. PLoS ONE 4(7): e6318. doi:10.1371/journal.pone.0006318

Editor: Tailoi Chan-Ling, University of Sydney, Australia

Received June 3, 2008; **Accepted** June 24, 2009; **Published** July 21, 2009

Funding: Part of this work was supported by grants from the Ministry of Education, Science, Sports and Culture, the Japanese Government; and from the Japan Ministry of Health, Labor and Welfare.

Competing Interests: The authors have declared that no competing interests exist.

* E-mail: kondo.yasushi@mc.mt-pharma.co.jp

Introduction

Embryonic stem (ES) cells, derived from the inner cell mass of blastocysts, are pluripotent cells that can differentiate into a variety of cell types including neural cells [1,2]. Among the various basic and clinical applications for ES cells, cell transplantation therapy for central nervous diseases is of particular interest because differentiated neurons do not proliferate, and a relatively large number of donor cells are necessary to replace diseased neurons. Several methods have been developed to prepare neural cells from ES cells. Neurons can be obtained indirectly from ES cells via ectodermal cells in embryoid bodies, which are formed from dissociated ES cells, either by induction with retinoic acid or selection [3,4]. Alternatively, neural stem cells and neurons can be directly differentiated from ES cells without forming embryoid bodies by culturing ES cells on mouse-cultured stroma cells (PA-6) [5], or under chemically defined low-density culture conditions [6]. All of these procedures, however, are time consuming and require highly complicated processes to generate many neurons. In addition, their practicality is limited by the possible teratogenicity caused by culture factors, such as retinoic acid, of differentiated cells. We have previously reported an efficient method to prepare transplantable neural cells from mouse ES cells using a conditioned medium collected from rat primary-cultured astrocytes (P-ACM) [7–9]. In this study, we applied this method to human ES (hES) cells for induction of neurons and astrocytes. Once the astrocytes were derived from hES cells, they could be substituted for primary astrocytes that induce neurons, thus achieving xeno-free production of neurons.

Results

Neural cell differentiation from hES

Four hES cell-lines stably expressing humanized renilla green fluorescent protein (hrGFP) were obtained. These hES cell-lines were kept in undifferentiated state with positive stem cell markers, such as alkaline phosphatase, Oct-4, and SSEA-4. When cultured

in P-ACM containing fibroblast growth factor-2 (FGF-2) under free-floating conditions, colonies of undifferentiated hES cells gave rise to floating spheres composed of neural stem cells and undifferentiated cells, which gradually increased in size during the culture. After 12 days of culture, the spheres were plated onto a poly-L-Lysine/Laminin coated dish and cultivated in neural stem cell medium (NSCM) containing high concentrations of FGF-2 and epidermal growth factor (EGF). Within 24 h, the spheres attached onto the substrate and formed circular clusters of cells. Many of these cells subsequently migrated to the surrounding areas and covered the growth surface of the dish in circular monolayers. After replacing NSCM by P-ACM and culture for 14 days, the spheres differentiated into neurons (Figures 1A, B) and few astrocytes (Figures 1C). These were identified by the neuronal marker tubulin β III isoform (Tuj1) and the astrocytic marker glial fibrillary acidic protein (GFAP).

Selective differentiation of hES cells into neurons and astrocytes

By culture of the spheres in NSCM, neural stem cells were able to migrate from the attached spheres to the surrounding area and subsequently form a circular cluster. NSCM containing FGF-2 and EGF promotes neural stem cells proliferation, while repressing their differentiation into any type of neural cells. After removing the core of the attached spheres mechanically, the remaining neural stem cells could proliferate in NSCM and selectively differentiate into neurons and astrocytes by subculture in an appropriate medium. To differentiate into neurons, neural stem cells were subcultured using 0.05% Trypsin/EDTA in P-ACM for 14 days (Figures 2A, B). After these 14 days of subculture, a large number of cells expressed Tuj1 ($84.0 \pm 5.1\%$, $n = 3$). On the other hand, to differentiate into astrocytes, neural stem cells were subcultured in G5 medium for 14 days (Figure 2C). After this subculture, a large number of cells expressed

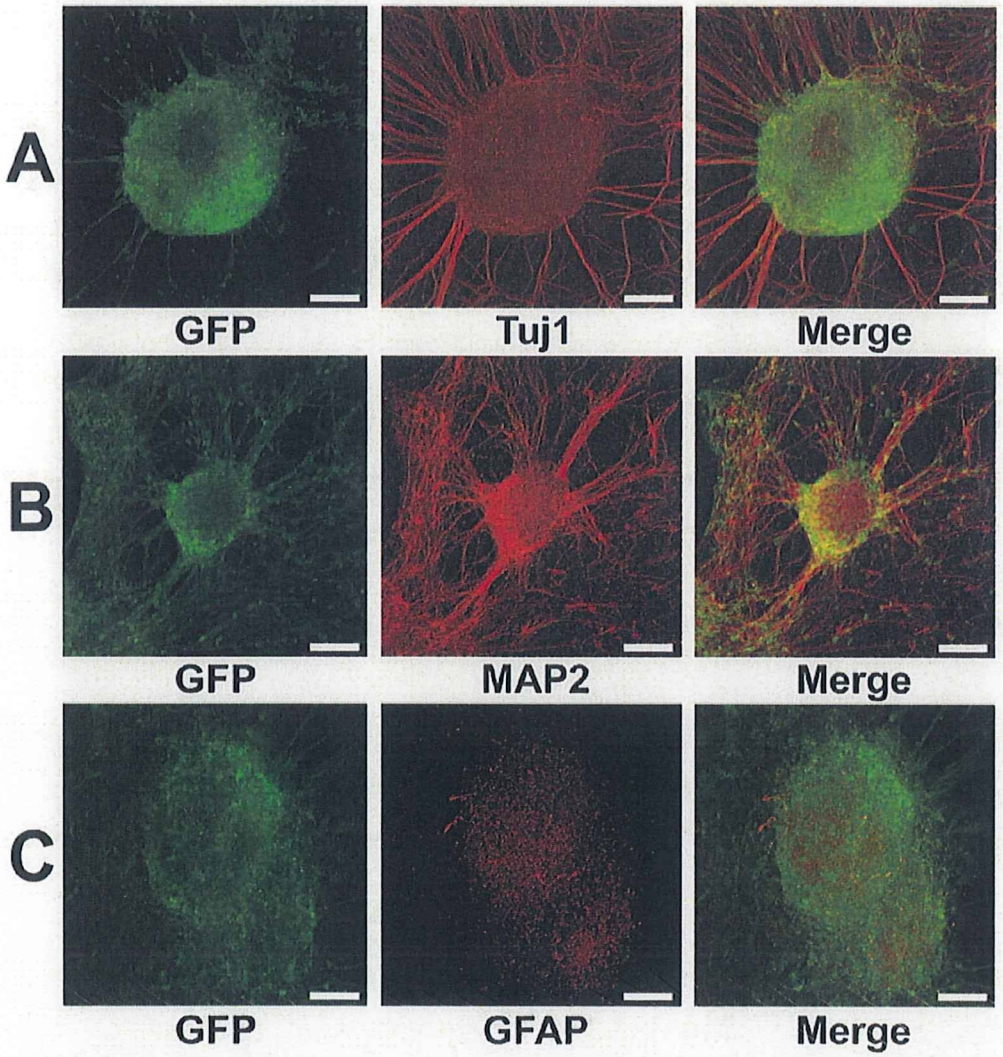

Figure 1. Differentiation of hES cells into neurons in P-ACM. Floating spheres composed of neural stem cells and undifferentiated cells grown for 12 days were plated on an adhesive substrate and cultured for 14 days in P-ACM. Expression of hrGFP (green), Tuj1 (A, red), MAP2 (B, red), and GFAP (C, red) staining of the many neural and few glial cells derived from hES cells. Bar = 100 μm.
doi:10.1371/journal.pone.0006318.g001

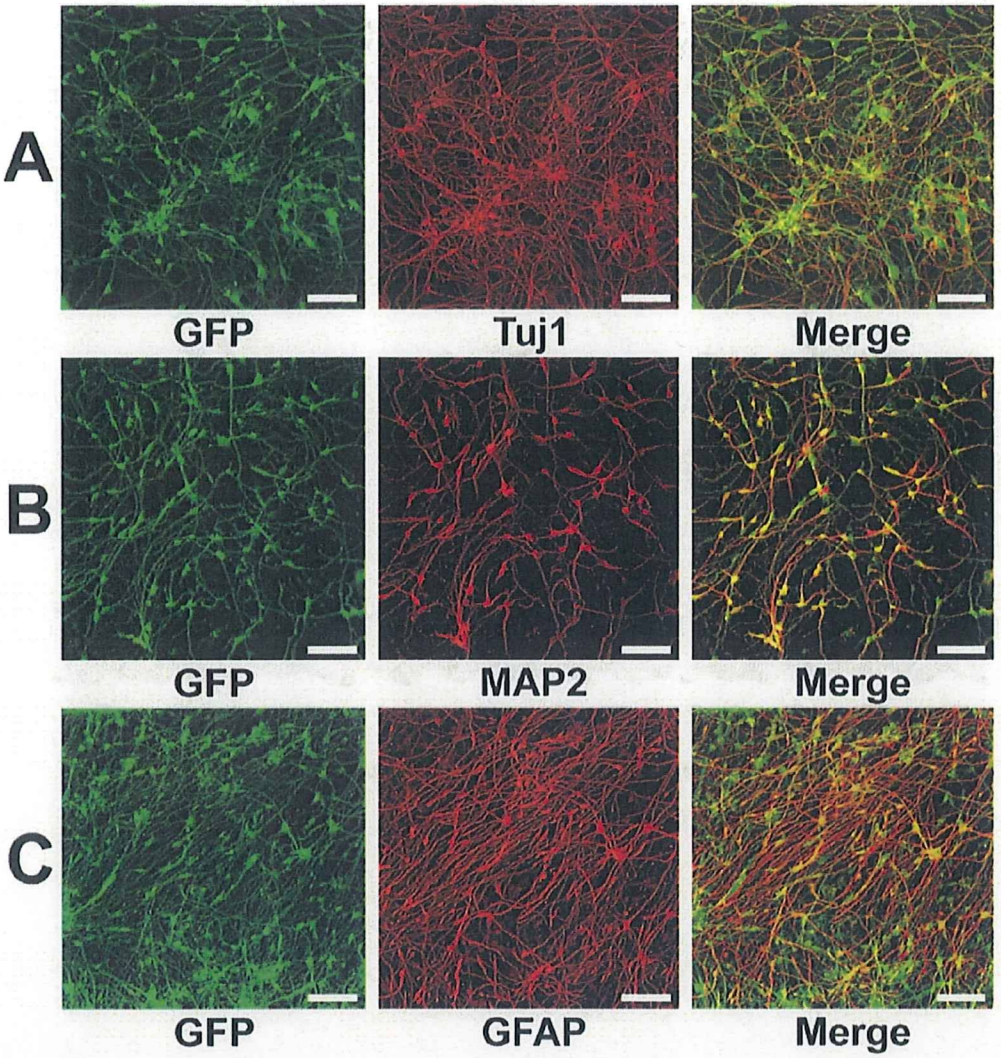

Figure 2. Selective induction of hES cells into neurons and astrocytes. (A, B): Neural stem cells that had migrated from floating spheres in NSCM were subcultured onto a PLL coated plate and cultured for 14 days in P-ACM. Immunostaining with antibody to Tuj1 and MAP2 showed that the subcultured neural stem cells had differentiated into neurons. Expression of hrGFP (green), (A) Tuj1 (red), and (B) MAP2 (red) staining profiles. (C): Neural stem cells were cultured for 14 days after removal of the core of spheres with a glass pipette and change of medium to G5 medium. The proliferated cells were subcultured onto PLL/LAM coated plate and cultured for 14 days in G5 medium. Immunostaining with antibody to GFAP showed that the subcultured cells had differentiated into astrocytes. Expression of hrGFP (green) and GFAP (red) staining profiles. Bar = 100 μm.
doi:10.1371/journal.pone.0006318.g002

GFAP (75.0±1.2%, $n = 3$). The removed core of the attached spheres could, like the first spheres, be used repeatedly (about twenty times) as seed for neural stem cells.

Xeno-free induction of astrocytes using a chemically defined medium

For collection of xeno-free astrocytes derived from hES cells, we used a chemically defined N2 medium for neural induction. When cultured in N2 medium containing FGF-2 and EGF under free-floating conditions, colonies of undifferentiated hES cells gave rise to floating spheres. As N2 was less efficient than P-ACM for obtaining astrocytes, we prepared hES cells in large scale ($>10^8$ cells). After differentiation, millions of astrocytes were gained under xeno-free condition (Figure 3A).

Neuronal induction of hES cell-derived astrocytes

Next, we investigated whether the astrocytes derived from hES cells can be substituted for primary astrocytes to differentiate hES cells into neural cells. A conditioned medium of hES cell-derived astrocytes was collected after two days culture and used as ES-ACM by adding an equal amount of N2 medium. As in the case of P-ACM, hES cells cultured in ES-ACM differentiated into neural cells via formation of spheres. After switching the cells from NSCM to ES-ACM, many cells had neuronal-like appearance with long neurites. By 6 weeks of culture in ES-ACM, most cells had neural morphology and expressed microtubule-associated protein 2 (MAP2) (Figure 3B). During our procedure for differentiating hES cells using ES-ACM, expression of several markers was analyzed by RT-PCR (Figure 4A). By 8 weeks culture

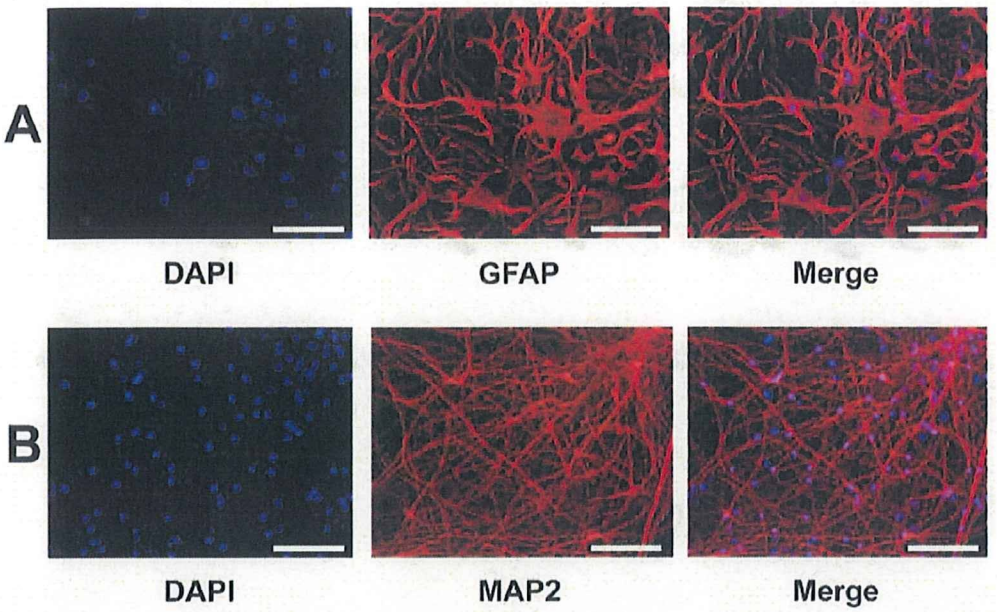

Figure 3. Differentiation of hES cells into astrocytes in a chemically defined medium. (A): Neural stem cells induced by N2 medium were cultured for 14 days after removal of the core of spheres with a glass pipette and change of medium to G5 medium. The proliferated cells were subcultured onto a PLL/LAM coated plate and cultured for 14 days in G5 medium. Immunostaining with antibody to GFAP showed that most of the subcultured cells had differentiated into astrocytes. DAPI (blue) and GFAP (green) staining profiles. Neural stem cells induced by xeno-free ES-ACM were subcultured onto PLL coated plate and cultured for 6 weeks in ES-ACM. (B): Immunostaining with antibody to MAP2 showed that the subcultured NSCs had differentiated into mature neurons. DAPI (blue) and MAP2 (red) staining profiles. Bar = 100 μm.
doi:10.1371/journal.pone.0006318.g003

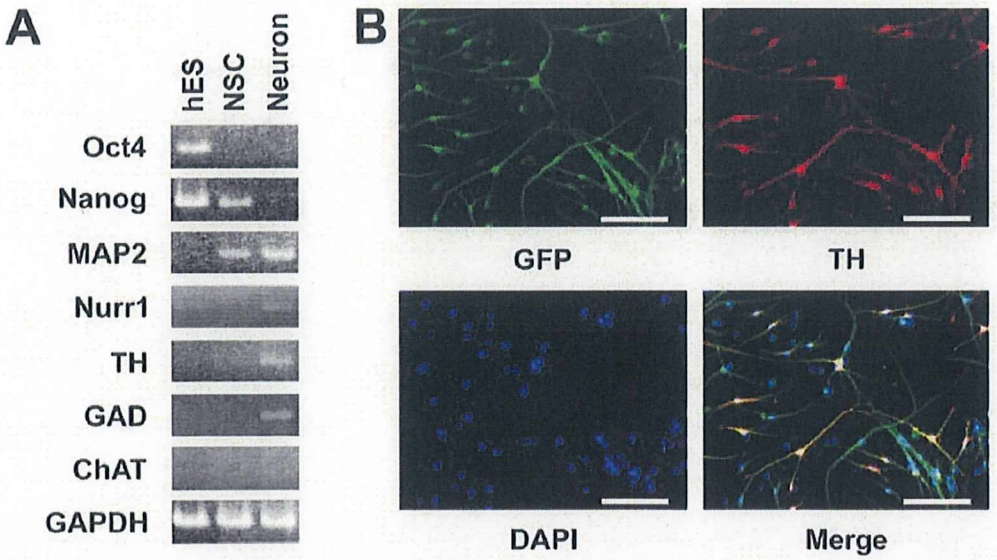

Figure 4. RT-PCR analysis and differentiation of hES cells into dopaminergic neurons in xeno-free ES-ACM. (A): RT-PCR analysis of hES cells, neural stem cells and mature neurons. RNA was isolated from clones of undifferentiated hES cells, from neural stem cells, and from mature neurons which had been cultured for 8 weeks in ES-ACM and analyzed for expression of marker genes. The expression levels of each gene were normalized to GAPDH gene expression level. hES, undifferentiated hES cells; NSC, neural stem cells; Neuron; mature neurons. (B): Differentiation of hES cells into dopaminergic neural cells in xeno-free ES-ACM. Neural stem cells induced by ES-ACM were subcultured onto PLL coated plate and cultured for 8 weeks in ES-ACM. Immunostaining with antibody TH and expression of hrGFP showed that the subcultured neural stem cells had differentiated into dopaminergic neurons. Expression of hrGFP (green), DAPI (blue) and TH (red) staining profiles. Bar = 100 μm.
doi:10.1371/journal.pone.0006318.g004

in ES-ACM, some cells showed tyrosine hydroxylase (TH) - immunoreactivity (Figure 4B). Furthermore, when cultured in ES-ACM again, the cells could differentiate into astrocytes via formation of spheres. To induce differentiation of neural stem cells into astrocytes, the culture medium was changed from NSCM to G5 medium. After medium change, most neural stem cells had the appearance of typical astrocytes. By 2 weeks culture in G5 medium, the majority (82.4±1.8%, $n=3$) of cells expressed GFAP, and few (<1%) expressed MAP2.

Electrophysiological analysis of neurons differentiated from hES cells

For electrophysiological study, hES-derived neurons were cultured on coverslips for 4–6 weeks. The coverslips were transferred to a recording chamber before use. Neurons were selected based on their appearance (spherical shape with long neurites). The resting membrane potential of the neurons were −62.0~−11.1 mV ($n=26$). Among 26 cells examined, action potentials were elicited in 22 cells (Figure 5A, Control). Application of 1 μM tetrodotoxin (TTX) completely suppressed the overshoot (Figure 5A, right panel). The action potentials were evoked only when resting membrane potentials were set to −70 mV by current injection in 11 cells. The rest of the cells did not possess membrane excitability ($n=4$ out of 26, closed circle in Figure 5B).

Survival of hES cell-derived neurons in mice brain

To examine differentiation of hES cell-derived cells *in vivo*, we transplanted neural stem cells induced with ES-ACM into mice brain ($n=7$). Before transplantation, the majority (85.1±5.1%, $n=4$) of donor cells expressed Nestin, a marker for neural stem cell (Figure 6A), and no cells expressed octamer transcription factor-3 (Oct-3) and stage-specific embryonic antigen (SSEA-4), two makers for undifferentiated cells (data not shown). Four weeks after engraftment, many ($2–3\times10^2$) hrGFP-positive cells were recognized (Figure 6B, C). Some of these cells (<10%) were also Tuj1-immunoreactive (Figure 6D). In the vicinity of the grafts, few cells were immunoreactive against Ki-67, a marker for proliferation. However, none of these Ki-67-positive cells were positive for hrGFP (Figure 6E). Teratoma was not detected in any of the transplanted mice.

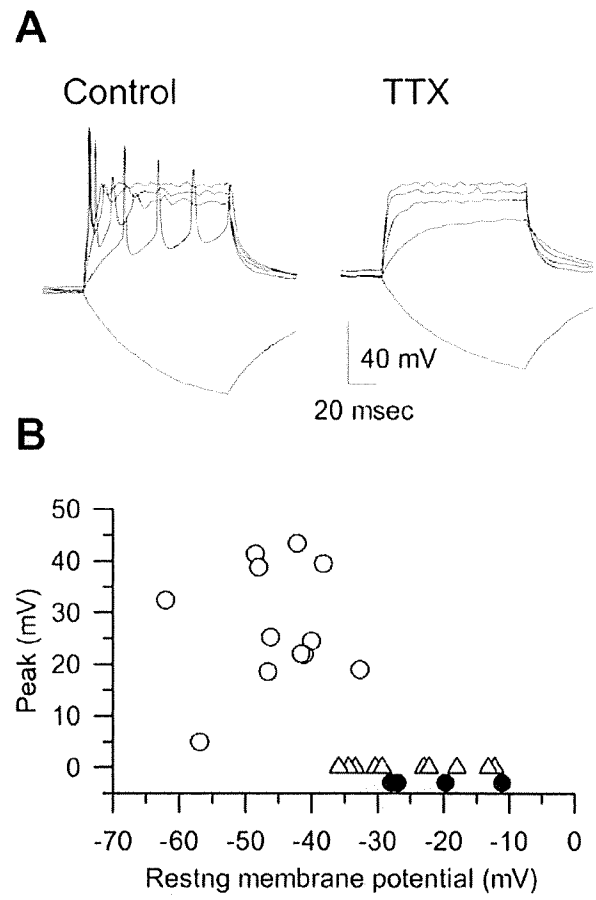

Figure 5. Electrophysiological properties of hES-derived neurons. (A): (Control) Action potentials elicited by depolarizing current injections (50 pA steps for 100 msec). The resting membrane potential was −62.0 mV. During the hyperpolarizing pulse (−50 pA), no 'sug' component was observed. (TTX) Membrane potentials recorded in the presence of 1 μM tetrodotoxin. In both panels, the dotted lines indicate 0 mV. (B): Summary of the resting membrane potentials and the peak amplitudes. Open circle; cells with action potentials. Open triangle; cells with action potentials only when the resting membrane potential was set to −70 mV. Closed circle; cells without membrane excitability.
doi:10.1371/journal.pone.0006318.g005

Discussion

We have shown in this study that neurons and astrocytes can be produced efficiently from hES cells using a conditioned medium collected from either rat primary-cultured astrocytes or hES cell-derived astrocytes. Astrocytes derived from hES cells can be used for continuous generation of neurons. Although a number of media including serum-free media supplemented with various cytokines and/or growth factors have been developed [10,11] to keep a long-term culture of neuronal cells, synthetic culture systems can usually maintain neural cells stable for only few weeks. Although a conditioned medium of primary-cultured astrocytes can be effective in culturing neurons for a longer period of time, the use of primary astrocytes may not be practical due to a number of limitations, including restricted availability of neural tissues as source of astrocytes, and extensive time and effort to obtain astrocytes from living tissues. Additionally, it is very difficult to maintain a stable culture of primary cells in a culture vessel, and subculture of these cells is limited within few passages.

The properties of primary-cultured astrocytes vary depending on the maturation stage of the living body and the region of the living tissue from which the astrocytes are derived. In addition, when astrocytes are obtained from a living body, contamination with cells other than the desired astrocytes is inevitable. Thus, it is difficult to prepare a stable astrocyte-conditioned medium having substantially uniform quality. With our method, on the other hand, ES-ACM can efficiently induce differentiation of hES cells into neural cells. Moreover, large amounts of ES-ACM can be produced stably and readily. ES-ACM, like P-ACM, can keep neuron cultures stable for more than eight weeks until mature neuronal phenotypes are apparent. In addition, completely xeno-free ES-ACM can be generated from immature hES cells by culture in chemically defined medium. With this completely xeno-free ES-ACM, xeno-free neurons and astrocytes can repeatedly be produced. In our transplantation experiment, donor cells did not express undifferentiated markers, such as Oct-3 and SSEA-4. In addition, only few Ki-67 positive cells found in the vicinity of the grafts were hrGFP-negative. These cells were unlikely to be derived from donor cells. It is important to exclude tumorigenicity of neuronal cells derived with this xeno-free method in future

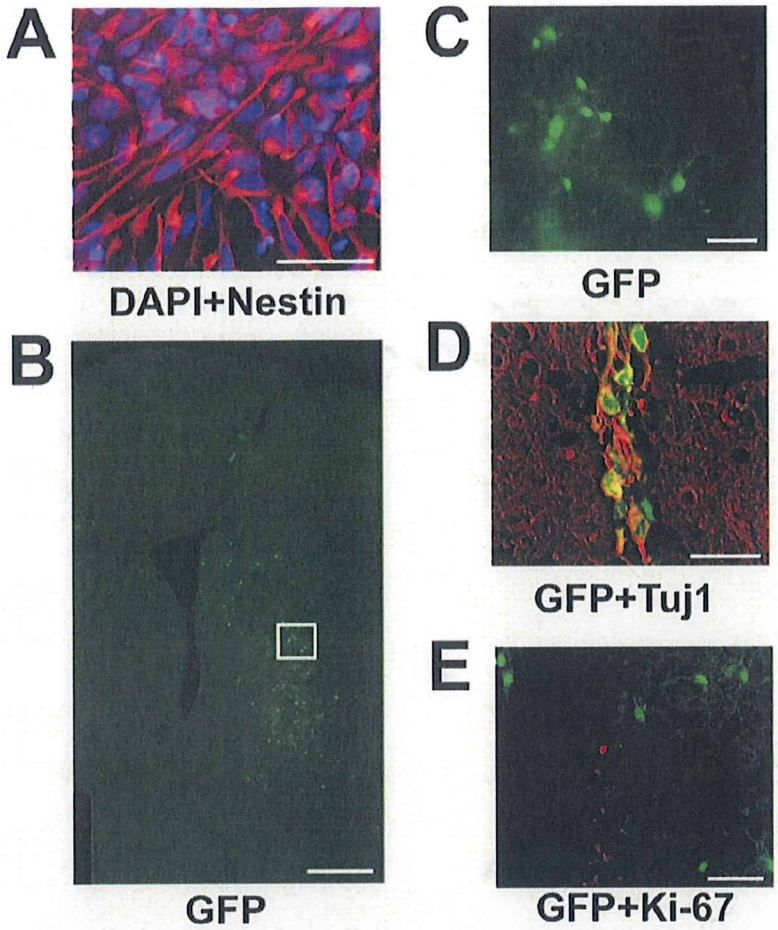

Figure 6. Survival of transplanted neural stem cells *in vivo*. (A): Most of the donor cells were confirmed to be Nestin-immunoreactve neural stem cells before transplantation. Anti-Nestin staining (green) and DAPI (blue). Bar = 50 μm. (B): Transplantation site. Grafted cells expressing hrGFP can be seen in the striatum. Bar = 500 μm. (C): High power magnification view of a white box in panel A. Some of the hrGFP-positive cells display a morphology similar to that of neurons. Bar = 50 μm. (D): Merged image of hrGFP expression (green) and immunostaining of anti-Tuj1 (red). Bar = 20 μm. (E): Merged image of hrGFP expression (green) and immunostaining of anti-Ki-67 (red). Bar = 50 μm.
doi:10.1371/journal.pone.0006318.g006

study for application to the cell therapy. Further studies are necessary to identify the specific molecules that induce neural cells in P- and ES-ACMs.

Recently, two methods adopting human tissue-derived cells have been reported as appropriate for clinical applications. One is an improved stromal cell-induced method that uses an amniotic membrane matrix [12]. The other uses telomerase-immortalized midbrain astrocytes [13]. Although both methods are xeno-free, they still need primary human tissues. On the other hand, with our method, neural cells can be induced from ES cells themselves. This self-serving method can supply donor cells consistently and may have an advantage for clinical applications.

Materials and Methods

ES cell culture

All experiments using hES cells were performed in conformity with "The Guidelines for Derivation and Utilization of Human Embryonic Stem Cells" of the Japanese government after approval by the institutional review board of Mitsubishi Tanabe Pharma Corporation. Two hES cell lines, SA002 and SA181, were obtained from Cellartis AB (Goteborg, Sweden) [14] and maintained on a mitotically inactivated mouse embryonic fibroblast feeder layer in a culture medium (vitroHES, Vitrolife AB, Goteborg, Sweden), supplemented with 4 ng/ml FGF-2 (Invitrogen, Carlsbad, CA). For passaging, the hES cells were treated with collagenase type IV (200 U/ml; Invitrogen) for 5 min, gently scraped from the culture dish, and then split 1:2–1:4 onto a feeder layer of mouse embryonic fibroblasts inactivated with 10 μg/ml mitomycin C.

Electroporation

All recombinant DNA experiments conformed to National Institute of Health (NIH) guidelines. First, a pGFP plasmid, in which hrGFP (Stratagene, La Jolla, CA) was expressed under the control of a CAG promoter (a gift from J. Miyazaki) [15] was constructed. Ten micrograms of the linearized plasmid was then electroporated into a suspension of hES cells (10^7 cells) in 0.8 mL of PBS using a Gene Pulser (500 μF, 250 V, Bio-Rad, Hercules, CA). The cells were next incubated on ice for 10 minutes, plated, and allowed to recover for 24 hours before selection with G418 (200 μg/mL). The cells were daily fed with the culture medium containing G418 for 12 days, after which the resulting ten G418-

resistant ES colonies showing strong hrGFP expression were individually picked and propagated. To analyze stem cell markers, alkaline phosphatase activity and cell surface markers were detected using an ES cell characterization kit (Chemicon, Temecula).

hES cell differentiation

Whole colonies of undifferentiated hES cells, 800–1000 μm in diameter, were picked up from the feeder layer using a glass capillary and transferred into non-adhesive bacteriological dishes each containing P-ACM supplemented with 20 ng/ml FGF-2 (R&D Systems Inc., Minneapolis). P-ACM was prepared as described previously [7]. The colonies were then cultured for 12 days, giving rise to spheres, which were next plated onto poly-L-Lysine/Laminin (Sigma-Aldrich, St. Louis) coated dishes and cultivated for seven days in NSCM (Neurobasal medium supplied with B27 supplement, both from Invitrogen, 20 ng/ml FGF-2, and 20 ng/ml recombinant EGF [R&D systems]). At this stage, the spheres gave rise to circular clusters of cells, many of which migrated from the clusters to the surrounding areas. After replacing the NSCM with P-ACM and culture for 14 days, the spheres differentiated into neurons and few astrocytes. To obtain more and purer neurons, the centers of the clusters containing undifferentiated ES cells were removed with a glass capillary, and the rest of the clusters were cultured for seven days in NSCM. Neuronal differentiation was then induced by subculture of neural stem cells using 0.05% Trypsin/EDTA in P-ACM for 14 days. To induce astrocytic differentiation, the neural stem cells were subcultured in G5 medium (Neurobasal medium supplemented with G5 supplement, both from Invitrogen, 10 ng/ml FGF-2, and 20 ng/ml EGF) for 14 days.

To induce astrocytic differentiation under xeno-free conditions, the colonies of hES cells were transferred into non-adhesive bacteriological dishes each containing N2 medium (Neurobasal medium supplied with N2 supplement, Invitrogen) supplemented with 20 ng/ml of FGF-2 and EGF. After the colonies were cultured for 12 days, few of them gave rise to spheres containing neural stem cells, which were subsequently plated onto poly-L-Lysine/Laminin in G5 medium. Centers of the spheres containing undifferentiated hES cells were removed with a glass capillary, and the rest of the clusters were cultured for seven days in G5 medium. By repeating over this cycle eight times, the spheres were purified to obtain pure neural stem cells. These neural stem cells were subcultured in G5 medium for 14 days to induce astrocytes. For collection of ES-ACM, hES cells derived-astrocytes were cultured in N2 medium for two days.

Immunostaining analysis

hES cells cultured in a 24-well plate were fixed in 4% paraformaldehyde in phosphate-buffered saline (PBS). Immunocytochemistry was performed using standard protocols and antibodies directed against Tuj1 (monoclonal 1:1000), MAP2 (monoclonal, 1:1000), GFAP (polyclonal 1:500), Oct-4 (monoclonal 1:500), SSEA-4 (monoclonal 1:400), Nestin (monoclonal 1:1000) (all from Chemicon), and TH (monoclonal, 1:400) (Acris Antibodies, Hiddenhausen, Germany). Alexa Fluor 594-labeled (Molecular Probes, Eugene, OR) and Cy3-labeled (GE healthcare, Uppsala, Sweden) secondary antibodies were used for visualization. 4′, 6-diamidino-2-phenylindole (DAPI, Kirkegaard Perry Laboratories, Gaithersburg) was used for nuclei staining.

Cell density of neural lineages (neurons and astrocytes) was determined by counting the numbers of DAPI, Tuj^+ and $GFAP^+$ cells per field at a magnification of 200 times using an inverted microscope. Five visual fields were randomly selected and counted for each sample. Numbers presented in figures represent the average percentage and SEM of positive cells over DAPI from three samples per each examination.

RT-PCR analysis

Total RNA was extracted from undifferentiated hES cells, neural stem cells, and neuronal cells using QIAshredder (QIAGEN, Hilden, Germany) and RNeasy Plus Mini kit (QIAGEN). Reverse transcription was carried out using random hexamers at 37°C for 60 minutes according to the manufacturer's instruction for First-Strand cDNA Synthesis Kit (GE Healthcare UK Ltd., Buckinghamshire, UK). PCR was carried out for 30 cycles using the specific primer sets. The reaction cycle was set at 95°C for 30 seconds, 55°C for 30 seconds, and 72°C for 30 seconds. The amplified fragments were subjected to electrophoresis in a 2% agarose gel, which was subsequently stained with ethidium bromide and photographed. The primers used are as follows: glyceraldelyde-3-phosphatedehydrogenase (GAPDH), ACCACAGTCCATGCCATCAC and TCCACCACCCTGTTGCTGTA; Oct4, CGTTCTCTTTGGAAAGGTGTTC and ACACTCGGACCACGTCTTTC; Nanog, AAGACAAGGTCCCGGTCAAG and CCTAGTGGTCTGCTGTATTAC; MAP2, CTTTCCGTTCATCTGCCATT and GCATATGCGCTGATTCTTCA; Nurr1, GCTAAACAAAACTTGCATGC and CTCATATCATGTGCCATACTAG; TH, GAGTACACCGCCGAGGAGATTG and GCGGATATACTGGGTGCACTGG; choline acetyltransferase (ChAT), ATGGGGCTGAGGACAGCGAAG and AAGTGTCGCATGCACTGCAGG; glutamic acid decarboxylase (GAD), ATTCTTGAAGCCAAACAG and TAGCTTTTCCCGTCGTTG.

Electrophysiology

The action potential was recorded using current clamp mode of Axopatch200B amplifier and Digidata 1320 interface (Axon, CA, USA). Physiological bathing solution contained (in mM); 140 NaCl, 5.4 KCl, 0.33 NaH_2PO_4, 0.5 $MgCl_2$, 1.8 $CaCl_2$, 5 HEPES (pH = 7.4 with NaOH). Standard high K^+ pipette solution contained; 110 Aspartic acid, 30 KCl, 5 MgATP, 5 Na_2 creatine phosphate, 0.1 Na_2GTP, 2 EGTA, 10 HEPES (pH = 7.2 with KOH). Electrode resistance was 8~6 MOhm. All experiments were carried out at 33–35°C.

Transplantation Experiment

Neural stem cells derived from hES cells using ES-ACM were implanted into the mouse striatum. All animal experimental protocols were approved by the Animal Ethics Committee of Mitsubishi Tanabe Pharma Corporation. 8-week-old C57BL/6 Cr Slc mice (SLC, Shizuoka, Japan) were anesthetized with pentobarbital and fixed on a stereotactic device (Narishige, Tokyo, Japan). By using a glass pipette with an inner diameter of 100 μm, 1×10^5 cells/5 μl were slowly (0.3 μl/min) injected into the striatum (AP±0 mm, ML +2.0 mm, DV −3.0 mm from bregma) of an adult male mouse. Four weeks after the transplantation, the recipient mouse was anesthetized with pentobarbital and perfused with ice-cold 4% paraformaldehyde in PBS. The brains of each mouse were postfixed in the same solution, cryoprotected with 30% sucrose in PBS for 48 h, and frozen. Coronal sections (thickness 40 μm) were cut on a microtome with freezing unit, collected in PBS (pH 7.4), and divided into series. Brain sections were incubated overnight with primary antibodies at 4°C. The primary antibodies used for immunohistochemistry ware mouse anti-Tuj1 (1:800, Covance, USA) and rabbit anti-Ki67 (1:25, abcam, UK). For detection of the primary antibodies, Alexa Fluor 594 goat anti-mouse IgG (1:1000; Molecular Probes) and Alexa

Fluor 594 goat anti-rabbit IgG (1:1000; Molecular Probes) were incubated with the samples. Immunoreactivity was assessed and viewed under confocal laser scanning microscopy (FV10i; Olympus, Tokyo).

Acknowledgements

We thank Jun-ichi Miyazaki, Osaka University Medical School, Osaka, Japan for the generous gift of plasmid pCAG. We also thank Naomi Takino and Hiroko Nishida, Division of Neurology, Department of Medicine, Jichi Medical University, Tochigi, Japan, for their technical assistance.

Author Contributions

Conceived and designed the experiments: TO HM SiM YK. Performed the experiments: TO NK HM KW MT. Analyzed the data: TO HM YS SN TI IN SiM MT YK. Contributed reagents/materials/analysis tools: TN SiM MT NI. Wrote the paper: TO SiM MT YK.

References

1. Thomson JA, Itskovitz-Eldor J, Shapiro SS, Waknitz MA, Swiergiel JJ, et al. (1998) Embryonic stem cell lines derived from human blastocysts. Science 282: 1145–1147.
2. Suemori H, Tada T, Torii R, Hosoi Y, Kobayashi K, et al. (2001) Establishment of embryonic stem cell lines from cynomolgus monkey blastocysts produced by IVF or ICSI. Dev Dyn 222: 273–279.
3. Bain G, Kitchens D, Yao M, Huettner JE, Gottlieb DI (1995) Embryonic stem cells express neuronal properties in vitro. Dev Biol 168: 342–357.
4. Okabe S, Forsberg-Nilsson K, Spiro AC, Segal M, McKay RD (1996) Development of neuronal precursor cells and functional postmitotic neurons from embryonic stem cells in vitro. Mech Dev 59: 89–102.
5. Kawasaki H, Mizuseki K, Nishikawa S, Kaneko S, Kuwana Y, et al. (2000) Induction of midbrain dopaminergic neurons from ES cells by stromal cell-derived inducing activity. Neuron 28: 31–40.
6. Tropepe V, Hitoshi S, Sirard C, Mak TW, Rossant J, et al. (2001) Direct neural fate specification from embryonic stem cells: a primitive mammalian neural stem cell stage acquired through a default mechanism. Neuron 30: 65–78.
7. Nakayama T, Momoki-Soga T, Inoue N (2003) Astrocyte-derived factors instruct differentiation of embryonic stem cells into neurons. Neurosci Res 46: 241–249.
8. Nakayama T, Momoki-Soga T, Yamaguchi K, Inoue N (2004) Efficient production of neural stem cells and neurons from embryonic stem cells. Neuroreport 15: 487–491.
9. Nakayama T, Sai T, Otsu M, Momoki-Soga T, Inoue N (2006) Astrocytogenesis of embryonic stem-cell-derived neural stem cells: Default differentiation. Neuroreport 17: 1519–1523.
10. Bottenstein JE, Sato GH (1979) Growth of a rat neuroblastoma cell line in serum-free supplemented medium. Proc Natl Acad Sci U S A 76: 514–517.
11. Brewer GJ, Cotman CW (1989) Survival and growth of hippocampal neurons in defined medium at low density: advantages of a sandwich culture technique or low oxygen. Brain Res 494: 65–74.
12. Ueno M, Matsumura M, Watanabe K, Nakamura T, Osakada F, et al. (2006) Neural conversion of ES cells by an inductive activity on human amniotic membrane matrix. Proc Natl Acad Sci U S A 103: 9554–9559.
13. Roy NS, Cleren C, Singh SK, Yang L, Beal MF, et al. (2006) Functional engraftment of human ES cell-derived dopaminergic neurons enriched by coculture with telomerase-immortalized midbrain astrocytes. Nat Med 12: 1259–1268.
14. Heins N, Englund MC, Sjoblom C, Dahl U, Tonning A, et al. (2004) Derivation, characterization, and differentiation of human embryonic stem cells. Stem Cells 22: 367–376.
15. Niwa H, Yamamura K, Miyazaki J (1991) Efficient selection for high-expression transfectants with a novel eukaryotic vector. Gene 108: 193–199.

Short Report

A convenient enzyme-linked immunosorbent assay for rapid screening of anti-adeno-associated virus neutralizing antibodies

Tetsuo Ito[1], Shigekazu Yamamoto[1], Tsukasa Hayashi[1], Mika Kodera[1,3], Hiroaki Mizukami[2], Keiya Ozawa[2] and Shin-ichi Muramatsu[3]

[1]KAINOS Laboratories Inc., Tokyo; [2]Division of Genetic Therapeutics; [3]Division of Neurology, Jichi Medical University, Tochigi, Japan
Corresponding author: Shin-ichi Muramatsu, 3311-1 Yakushiji, Shimotsuke, Tochigi 329-0498, Japan. Email: muramats@jichi.ac.jp

Abstract

Background: Recombinant adeno-associated virus vectors based on serotype 2 (AAV-2) have become leading vehicles for gene therapy. Most humans in the general population have anti-AAV-2 antibodies as a result of naturally acquired infections. Pre-existing immunity to AAV-2 might affect the functional and safety consequences of AAV-2 vector-mediated gene transfer in clinical applications.

Methods: An enzyme-linked immunosorbent assay (ELISA) method was developed using microwell plates coated with intact particles of recombinant AAV-2 vectors, and horseradish peroxidase-conjugated anti-human immunoglobulin G (HRP-IgG). Neutralizing antibody titres were analysed by assessing the ability of serum antibody to inhibit transduction into HEK293 cells of AAV vectors that express β-galactosidase.

Results: Anti-AAV-2 antibodies were detected by ELISA in two of 20 healthy subjects. The positivity criterion (optical density >0.5) in ELISA corresponded to the cut-off value (320-fold dilution of serum) in the AAV-2 neutralization assay. Influences of interfering substances were not observed.

Conclusion: This ELISA method may be useful for rapid screening of anti-AAV-2 neutralizing antibodies in candidates for gene therapy.

Ann Clin Biochem 2009; 46: 508–510. DOI: 10.1258/acb.2009.009077

Introduction

Adeno-associated virus (AAV) is a small single-stranded DNA virus within the parvovirus family.[1,2] Among more than 100 genotypes of primate AAV, serotype 2 (AAV-2) is the most studied and was the first to be engineered for vector development. Recombinant AAV-2 vectors efficiently transduce both dividing and non-dividing cells and provide long-term gene expression without significant toxicity. Growing numbers of clinical trials have been conducted using AAV-2 vectors to combat various diseases. However, one major problem is the high prevalence of anti-AAV-2 antibodies in the human population. More than 90% of adults demonstrate antibodies that cross-react with one or more AAV serotypes, although markedly fewer (18–32%) show neutralizing antibodies (nAb).[3,4] Pre-existing immunity to AAV-2 may block transduction and intensify the innate response to vector administration, leading to a poor outcome of gene therapy. Thus, measurement of the anti-AAV-2 nAb titre is necessary.

Methods

Recombinant AAV-2 vectors were produced by the triple transduction method as described previously.[5] In brief, HEK293 cells were transfected with the following three plasmids: pAAV2-Rep/vp (containing the AAV-2 *rep* and *cap* genes), pAd (containing the adenovirus genome) and pW1 (containing the β-galactosidase-expression cassette). After three days of incubation, the transfected cells were frozen and thawed, and the recombinant AAV-2 vector particles that were released were purified by two sequential CsCl density gradient centrifugations.

Serum samples from healthy adults were purchased from Advanced BioServices LLC, (Reseda, CA, USA). AAV-specific antibodies were detected using an enzyme-linked immunosorbent assay (ELISA). Ninety-six-well microtitre plates (Invitrogen, Carlsbad, CA, USA) were coated with 0.5 μg (1.4×10^8 vector genomes [vg]) of AAV-2 vector particles per well. After blocking with 2% bovine serum albumin (BSA) in phosphate-buffered saline (PBS), the plates were washed with 2% sucrose. Serum samples diluted at 1:1000 with PBS/0.1% BSA were added to each well (100 μL/well). The plates were incubated for 1 h at room temperature (RT) and washed three times with PBS/0.05% Tween 20. A solution containing 1 μg/mL horseradish peroxidase-conjugated anti-human immunoglobulin G (HRP-IgG; self-prepared using a heterobifunctional

reagent) was added to each well (100 μL/well). The plates were incubated for 1 h at RT and washed three times with washing buffer. Colour was developed by adding 100 μL 3,3′,5,5′-tetramethylbenzidine/urea hydrogen peroxide (Neogen, Lexington, KY, USA) and incubating the plates for 30 min at RT. Colour development was stopped by adding 1 mol/L sulphuric acid (100 μL/well), and the optical density (OD) was measured at 450/640 nm. The optimum reaction conditions were determined in the following ranges: 0.5×10^8 to 3×10^8 vg of AAV-2 vector particles per well, 10- to 5000-fold dilution of the specimen and 0.01–0.4 μg/mL concentration of HRP-IgG. The effects of bilirubin, haemoglobin and chyle as endogenous interference materials were studied. Samples including these materials at 500 mg/L, 5000 mg/L and 3000°, respectively, were mixed with sera at a volume ratio of 1 : 9 and analysed by ELISA.

For the nAb assay, sera were continuously diluted two-fold with Dulbecco's Modified Eagle's Medium and Harn's F-12 Nutrient Mixture (DMEM/F12, Invitrogen) 10% fetal bovine serum (Sigma-Aldrich, St. Louis, MO, USA), 100 U/mL penicillin (Invitrogen) and 100 μg/mL streptomycin (Invitrogen). AAV-2 vectors were diluted with 10 mmol/L HEPES/130 mmol/L NaCl (pH 8.0) up to 1.4×10^8 vg/μL, and optimum transduction was obtained with 1.4×10^{10} vg/μL. Ten microlitres of diluted serum were added to 5 μL diluted AAV-2 vector, and the mixture was incubated for 1 h at RT. The mixture was then added to 96-well plates containing confluent HEK293 cells. Two days after transduction, β-galactosidase activity was measured with a β-galactosidase assay kit (Invitrogen). The titre of nAb was defined as the highest dilution of serum that showed <50% of the β-galactosidase activity of the negative control.

Results and discussion

In the ELISA method developed in this study, AAV-2 vector particles immobilized on plates captured AAV-2-specific antibodies. Using whole vector particles as antigens without degradation, antibodies that are more specific AAV-2, including nAb, can be assessed. Intra-assay precision was determined by repeatedly ($n = 8$) measuring four kinds of serum with different nAb titres. For three samples whose nAb titres were ×640, ×80 and ×80, the coefficient of variation (CV) of the OD was 2.5%, 4.3% and 1.8%, respectively. For the fourth sample, with ×10 titre, the average OD was 0.012 and the CV was 8.5%. These data confirm the good precision of the assay. The effects of interference materials were <10%, suggesting that the method had good specificity. All reagents, including AAV particles, were stable after storage for 13 months at 4°C, and sensitivity of the ELISA was maintained at 95% with fresh reagents.

The nAb titres for 20 healthy donor samples varied from ×10 to ×640, and 13 samples had a titre less than ×20. Using the ELISA method, the absorbance values of the samples varied from 0.012 to 0.752, and 15 samples showed absorbance of less than 0.08 (Table 1). In our study, a nAb titre higher than × 32 corresponded to an OD greater than 0.5 in the ELISA. If these values were used as cut-off points, two of 20 samples found to be positive in both the nAb assay and the ELISA. Further studies on more samples were necessary to validate the cut-off values in different populations.

Table 1 Correlation between a neutralizing antibody assay (nAb) and the ELISA method

	nAb assay		ELISA	
Sample ID	nAb titre	Decision	OD	Decision
1	10	Neg.	0.014	Neg.
2	80	Neg.	0.075	Neg.
3	10	Neg.	0.013	Neg.
4	10	Neg.	0.016	Neg.
5	160	Neg.	0.291	Neg.
6	80	Neg.	0.015	Neg.
7	80	Neg.	0.032	Neg.
8	10	Neg.	0.010	Neg.
9	10	Neg.	0.025	Neg.
10	10	Neg.	0.012	Neg.
11	10	Neg.	0.014	Neg.
12	80	Neg.	0.468	Neg.
13	10	Neg.	0.012	Neg.
14	320	Pos.	0.596	Pos.
15	640	Pos.	0.725	Pos.
16	10	Neg.	0.013	Neg.
17	20	Neg.	0.114	Neg.
18	10	Neg.	0.046	Neg.
19	10	Neg.	0.016	Neg.
20	10	Neg.	0.012	Neg.

OD, optical density; ELISA, enzyme-linked immunosorbent assay; nAb, neutralizing antibodies

AAV-2 antibody in 20 sera from healthy individuals was analysed by ELISA and a neutralizing antibody assay. The measured values were expressed as OD or titre. The cut-off value for the neutralizing antibody assay was provisionally fixed at ×320. The criterion for positivity for the ELISA method was considered greater than OD 0.5

Conclusion

We have developed a simple and convenient ELISA method for detecting serum anti-AAV-2 antibodies. Antibody titres assessed by this method show good correlation with nAb titres obtained in a cell transduction assay, suggesting that this ELISA may be useful for the rapid screening of nAbs in candidates for gene therapy.

DECLARATIONS

Competing interests: None.

Funding: Part of this work was supported by a grant (19591003) from the Ministry of Education, Science, Sports and Culture of the Japanese Government, and a grant (20261501) from the Japan Ministry of Health, Labour and Welfare.

Ethical approval: The ethics committee of Jichi Medical University approved this study (GT-001).

Guarantor: SM.

Contributorship: Conceived and designed the experiments: SM, HM, TI, TH. Performed the experiments: TY, MK, HM, Analysed the data: TI, SY, TH, MK, HM, KO, SM, Wrote the paper: TI, SM.

REFERENCES

1 Gao G, Vandenberghe LH, Alvira MR, *et al.* Clades of adeno-associated viruses are widely disseminated in human tissues. *J Virol* 2004;78:6381–8
2 Wu Z, Asokan A, Samulski RJ. Adeno-associated virus serotypes: vector toolkit for human gene therapy. *Mol Ther* 2006;**14**:316–27
3 Chirmule N, Propert K, Magosin S, *et al.* Immune responses to adenovirus and adeno-associated virus in humans. *Gene Ther* 1999;6:1574–83
4 Moskalenko M, Chen L, van Roey M, *et al.* Epitope mapping of human anti-adeno-associated virus type 2 neutralizing antibodies: implications for gene therapy and virus structure. *J Virol* 2000;74:1761–6
5 Li XG, Okada T, Kodera M, *et al.* Viral-mediated temporally controlled dopamine production in a rat model of Parkinson disease. *Mol Ther* 2006;**13**:160–6

(Accepted 24 June 2009)

THE JOURNAL OF BIOLOGICAL CHEMISTRY VOL. 284, NO. 47, pp. 32895–32905, November 20, 2009

Isolation and Characterization of Patient-derived, Toxic, High Mass Amyloid β-Protein (Aβ) Assembly from Alzheimer Disease Brains*[S]

Received for publication, March 2, 2009, and in revised form, September 10, 2009 Published, JBC Papers in Press, September 15, 2009, DOI 10.1074/jbc.M109.000208

Akihiko Noguchi,[a] Satoko Matsumura,[a] Mari Dezawa,[b,c] Mari Tada,[d] Masako Yanazawa,[a] Akane Ito,[a] Manami Akioka,[a] Satoru Kikuchi,[a] Michio Sato,[a] Shouji Ideno,[e] Munehiro Noda,[e] Atsushi Fukunari,[e] Shin-ichi Muramatsu,[f] Yutaka Itokazu,[b] Kazuki Sato,[g] Hitoshi Takahashi,[d] David B. Teplow,[h] Yo-ichi Nabeshima,[b] Akiyoshi Kakita,[d] Kazutomo Imahori,[i] and Minako Hoshi[a,b1]

From the [a]Mitsubishi Kagaku Institute of Life Sciences, Tokyo 194-8511, Japan, [b]Kyoto University, Kyoto 606-8501, Japan, [c]Tohoku University, Sendai 908-8575, Japan, [d]Niigata University, Niigata 951-8585, Japan, [e]Mitsubishi Tanabe Pharma Corporation, Osaka 541-8505, Japan, [f]Jichi Medical University, Tochigi 329-0498, Japan, [g]Fukuoka Women's University, Fukuoka 813-8529, Japan, the [h]David Geffen School of Medicine, UCLA, Los Angeles, California 90095, and [i]University of Tokyo, Tokyo 113-8654, Japan

Amyloid β-protein (Aβ) assemblies are thought to play primary roles in Alzheimer disease (AD). They are considered to acquire surface tertiary structures, not present in physiologic monomers, that are responsible for exerting toxicity, probably through abnormal interactions with their target(s). Therefore, Aβ assemblies having distinct surface tertiary structures should cause neurotoxicity through distinct mechanisms. Aiming to clarify the molecular basis of neuronal loss, which is a central phenotype in neurodegenerative diseases such as AD, we report here the selective immunoisolation of neurotoxic 10–15-nm spherical Aβ assemblies termed native amylospheroids (native ASPDs) from AD and dementia with Lewy bodies brains, using ASPD tertiary structure-dependent antibodies. In AD patients, the amount of native ASPDs was correlated with the pathologic severity of disease. Native ASPDs are anti-pan oligomer A11 antibody-negative, high mass (>100 kDa) assemblies that induce degeneration particularly of mature neurons, including those of human origin, *in vitro*. Importantly, their immunospecificity strongly suggests that native ASPDs have a distinct surface tertiary structure from other reported assemblies such as dimers, Aβ-derived diffusible ligands, and A11-positive assemblies. Only ASPD tertiary structure-dependent antibodies could block ASPD-induced neurodegeneration. ASPDs bind presynaptic target(s) on mature neurons and have a mode of toxicity different from those of other assemblies, which have been reported to exert their toxicity through binding postsynaptic targets and probably perturbing glutamatergic synaptic transmission. Thus, our findings indicate that native ASPDs with a distinct toxic surface induce neuronal loss through a different mechanism from other Aβ assemblies.

Neurodegenerative diseases, such as Alzheimer disease (AD),[2] Parkinson disease, prion diseases, and the polyglutamine diseases, arise from abnormal protein interactions in the central nervous system (1). In these diseases, complex multistep processes of protein conformational change and accretion produce various nonfibrillar assemblies, leading finally to fibrils (1–5). Recent studies have suggested that the early assemblies in this process might be the most toxic, possibly through the exposure of buried moieties and the formation of surface tertiary structures not present in physiologic monomers (6). These surface tertiary structures could mediate abnormal interactions with other cellular components (1).

In AD, extensive studies have suggested that accumulation of amyloid β-protein (Aβ), a physiologic derivative of amyloid precursor protein (APP), plays a primary pathogenic role (7–9). Various forms of assemblies ranging in mass from dimers up to multimers of ~1 MDa have been reported as neurotoxins (10–13) as follows: protofibrils (14); dimers/trimers (natural low-*n* oligomers) (15); 3–24-mer Aβ-(1–42) assemblies termed Aβ-derived diffusible ligands (ADDLs) (16); 12-mers termed globulomers (17) or Aβ*56 (18); 15–20-mer Aβ assemblies termed Aβ oligomers (AβOs) (19); and 150-mer or higher assemblies termed β-sheet intermediates (20). Whether or not they share a common surface, the tertiary structure responsible

* This work was supported in part, by National Institutes of Health Grant NS038328 (to D. B. T.), by Health and Labour Sciences Research Grants "Research on Nanotechnical Medical" (to M. H.) and "Research on Psychiatric and Neurological Diseases and Mental Health" (to M. D.) from the Ministry of Health, Labor, and Welfare, by Special Coordination Funds for Promoting Science and Technology (to M. H.) from the Ministry of Education, Culture, Sports, Science, and Technology, and by the Program for Promotion of Fundamental Studies in Health Sciences (to M. D.) from the National Institute of Biomedical Innovation The authors declare the following conflict of interest: this work was supported in part by a grant (to M. H.) from Mitsubishi Kagaku Institute of Life Sciences, which is a nonprofit organization financially supported by Mitsubishi Chemical Corp.; this grant expires in March 2009.

[S] The on-line version of this article (available at http://www.jbc.org) contains supplemental Experimental Procedures, Tables S1 and S2, Figs. S1–S7, and additional references.

[1] To whom correspondence should be addressed: Sakyo-ku, Kyoto 606-8501, Japan. E-mail: minhoshi@lmls.med.kyoto-u.ac.jp.

[2] The abbreviations used are: AD, Alzheimer disease; Aβ, amyloid β-protein; APP, amyloid precursor protein; sAPPα, human secreted form of APP; ADDL, Aβ-derived diffusible ligand; AβO, Aβ oligomer; ASPD, amylospheroid; DLB, dementia with Lewy bodies; MALDI-TOF/MS, matrix-assisted laser desorption/ionization time-of-flight mass spectrometry; HFIP, 1,1,1,3,3,3-hexafluoro-2-propanol; PBS, Dulbecco's phosphate-buffered saline without Ca^{2+} and Mg^{2+}; TEM, transmission electron microscopy; IP, immunoprecipitation; NCI, noncognitively impaired; MSCs, bone marrow stromal cells; NMDA-R, *N*-methyl-D-aspartate-type glutamate receptor; DIV, days *in vitro*; NCI, noncognitively impaired.

for toxicity remains unsettled; some of these assemblies are detected by specific antibodies (17, 21), whereas others are detected by a polyclonal A11 antibody (18, 19) that is reported to recognize epitopes associated with a certain oligomer state of amyloids regardless of their amino acid sequence (22). However, these assemblies, which differ in origin, mass, and toxic activity, mostly bind to postsynapses, leading to synaptic impairment (17–19, 23, 24). They are also suggested to play a role in synaptic impairment in AD model mice carrying human APP (17, 18, 25), which retain early features of AD such as amyloid plaques, synaptic loss, and mild memory deficits (26, 27). These observations collectively suggest that these assemblies play a role in AD pathogenesis by causing synaptic impairment. On the other hand, it remains largely unknown how, after the synaptic impairment, these assemblies cause subsequent neuronal loss in human AD brains. One reason is that no overt neuronal cell loss has been observed in most APP transgenic mice (except APP23 mice (28, 29)), even in the presence of these assemblies (26, 27). Another reason is that, as for the nonfibrillar Aβ assemblies actually present in human AD brains, Aβ dimers that induce synaptic impairment and not neuronal loss were recently isolated (30), but Aβ assemblies that directly cause neuronal loss have not yet been isolated either from AD patients or from the mice. Because soluble fractions of brains from humans with AD have been reported to contain Aβ assemblies ranging in size from dimers to polymers larger than 100 kDa (31), which appear to correlate with dementia (32, 33), Aβ assemblies responsible for neuronal loss might be present in the soluble fractions of AD brains. As has recently been shown clinically and diagnostically (34–37), neuronal loss plays an important role in cognitive deterioration of AD patients, so we aimed to isolate toxic Aβ assemblies from the soluble fractions of AD brains.

As a first step to isolate such Aβ assemblies *in vivo*, we have previously prepared highly toxic spherical Aβ assemblies termed "amylospheroids" (ASPDs) *in vitro* (38). Notably, ASPDs are considered not to be intermediates in the pathway leading to fibrils, because ASPDs were not incorporated into mature fibrils and continued to exist after fibril formation (13, 38). They also differ from protofibrils and ADDLs in morphology and size (11, 13, 38).

Here, we generated ASPD tertiary structure-dependent antibodies and used them to selectively immunoisolate a human counterpart of ASPDs (native ASPDs) from patients with AD or dementia with Lewy bodies (DLB). To distinguish native ASPDs from *in vitro*-produced ASPDs, the latter is hereafter referred to as synthetic ASPDs. Native ASPDs are A11-negative, high mass Aβ assemblies that induce degeneration of human neuronal cells *in vitro*, particularly those with mature character, and they differ in mass, surface tertiary structure, and neurotoxicity mechanism from other reported nonfibrillar Aβ assemblies (summary in supplemental Table S1).

EXPERIMENTAL PROCEDURES

Aβ Source—Aβ-(1–40) peptides were synthesized using *N*-(9-fluorenyl)methoxycarbonyl (Fmoc) chemistry on an Applied Biosystems model 433A peptide synthesizer and purified (38). Their structure and purity were confirmed using quantitative amino acid analysis, analytic high pressure liquid chromatography, and matrix-assisted laser desorption/ionization-time-of-flight/mass spectrometry (MALDI-TOF/MS; Ultraflex II, Bruker Daltonics). The purified Aβ-(1–40) was lyophilized, dissolved in 35% (v/v) acetonitrile in 0.1% (v/v) trifluoroacetic acid (~50 nmol/tube), and lyophilized. This step was repeated twice. Aβ-(1–42) peptides (25 mg/ampoule; Bachem lots 0552992 and 1000255) were completely dissolved in ~54 ml of 1,1,1,3,3,3-hexafluoro-2-propanol (Aldrich) by incubating the peptide solution overnight at 4 °C and then for 3 h at 37 °C and finally lyophilized (~40 nmol/tube). This step was repeated two or three times. The lyophilized peptides were kept at −20 °C.

Preparation and Purification of Synthetic ASPDs—Synthetic ASPDs were prepared *in vitro* either from 50 μM solution of Aβ-(1–40) (0.5× Dulbecco's phosphate-buffered saline without Ca^{2+} and Mg^{2+} (PBS); Nissui Pharmaceutical Co. Ltd.) or of Aβ-(1–42) (either 0.5× PBS or F12 buffer without L-glutamine and phenol red) by slowly rotating the solution (5–7 days for Aβ-(1–40); 14 h for Aβ-(1–42)), as described previously (38). At concentrations below a critical fibril-forming concentration (~100 μM) (39), spherical Aβ assemblies (5–20 nm in diameter for Aβ-(1–40); 5–25 nm for Aβ-(1–42); >85% 10–15 nm spheres), with rare fibril-like structures, were usually produced. The most toxic ASPDs (prepared either from Aβ-(1–40) or Aβ-(1–42)) were previously identified as 10–15-nm spheres recovered by glycerol gradient centrifugation in the fraction migrating near the thyroglobulin (669 kDa) standard (38). Further analysis of standard proteins using this glycerol gradient sedimentation assay revealed that the mass of the most toxic ASPDs is approximately equal to that of aldolase (158 kDa) but does not exceed that of thyroglobulin (669 kDa).[3] Therefore, the most toxic ASPDs were purified as retentates by using 100-kDa molecular mass cutoff filters (Ultrafree-MC, Millipore) to remove lower mass Aβ assemblies. In some experiments, including mature neuron-binding assays, the most toxic ASPD fraction was also purified by two-step filtrations (see Scheme 1). Studies using transmission electron microscopy (TEM) revealed that 10–15-nm spheres were predominantly recovered in the most toxic ASPD fraction (termed "158–669-kDa ASPDs") that passed through 0.22-μm filters but were retained on 100-kDa molecular mass cutoff filters (data not shown). Although these 10–15-nm spheres were hardly detectable in 100-kDa filtrates, smaller particles with a diameter of 5–6 nm were present in 100-kDa filtrates. A very small amount of 10–15-nm ASPDs was also present in 0.22-μm retentates because they remained bound to the filter (data not shown). These TEM observations were in good agreement with the results of dot blots and toxicity assays shown in Fig. 1*A*. Quantitative amino acid analysis revealed that generally ~25% of total Aβ was recovered as 158–669-kDa ASPDs. Synthetic ASPDs were prepared every week, and their quality was confirmed using dot blotting, TEM, and toxicity assays. Aβ concentration of each preparation was deter-

[3] A. Noguchi and M. Hoshi, unpublished data.

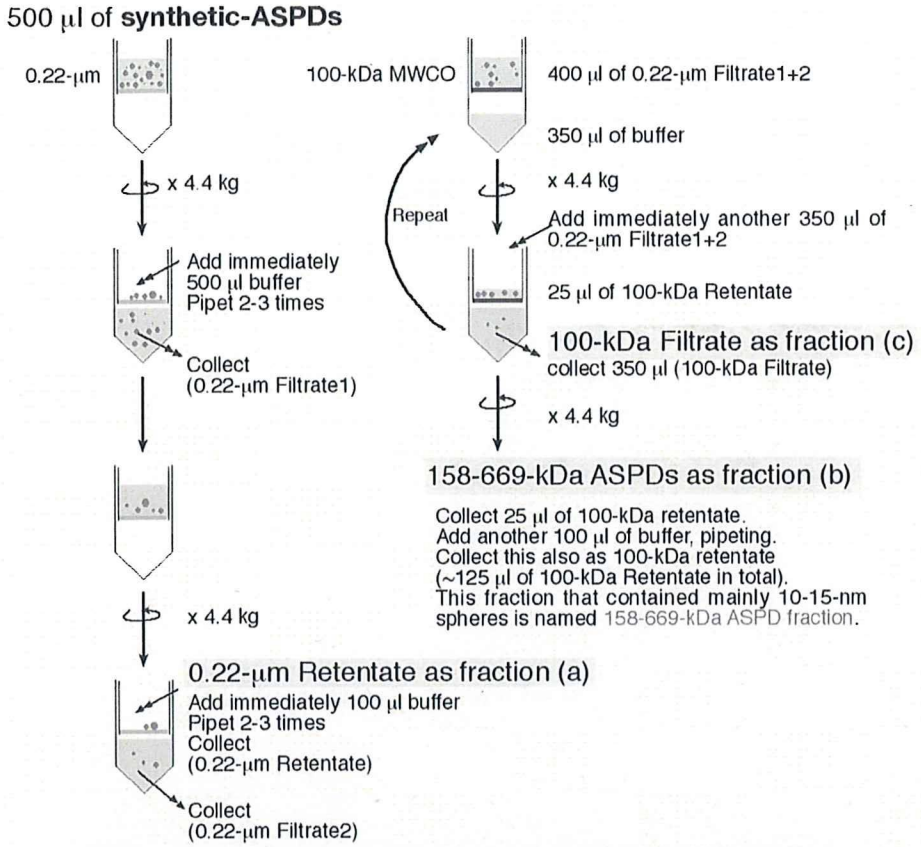

SCHEME 1. **Fractionation of the most toxic 158–669-kDa ASPDs by two-step filtrations.**

mined every week by quantitative amino acid analysis (Waters AccQ-Tag system) (38).

Preparation of Aβ Monomers and Fibrils—To prepare monomers, Aβ-(1–40) or Aβ-(1–42) lyophilizates were solubilized to 50 μM in 1,1,1,3,3,3-hexafluoro-2-propanol. The solution was incubated for 30 min at room temperature and then centrifuged at 20,400 × *g* for 30 min at 4 °C, and the upper 90% of the supernatant volume was collected. The monomer concentration was determined by means of quantitative amino acid analysis (38). To produce fibrils, Aβ-(1–40) was dissolved at a concentration of 100 μM in 0.5× PBS, pH 3.5. This solution was incubated without agitation at 37 °C for 2 days, after which fibrils were separated from the monomer and low mass Aβ assemblies by filtration through 100-kDa molecular mass cutoff filters. Large amounts of fibrils without ASPDs were detected reproducibly by TEM. The fibril concentration was determined by means of quantitative amino acid analysis (38). To obtain different types of fibrils for immuno-TEM analysis, fibrils were also produced by slowly rotating the above Aβ-(1–40) solution or by dissolving Aβ-(1–40) at a concentration of 350 μM in PBS, pH 7.5, followed by incubation for 5–7 days at 37 °C, with or without slow rotation (38).

Preparation of Aβ Oligomers for A11 Antibody—A test membrane, on which soluble Aβ oligomers (termed AβOs) and Aβ fibrils (1–3 μg/dot) were spotted, was produced by Dr. C. Glabe (University of California, Irvine) according to reported methods (22, 40). This test membrane was kindly provided by Invitrogen as a positive control for A11 antibody.

Preparation of ADDLs—ADDLs were produced as described previously (16). Aβ-(1–42) lyophilizates were solubilized to 5 mM in DMSO, diluted to 100 μM with F12, and incubated for 24 h at 4 °C. The solution was centrifuged at 14,000 × *g* for 10 min at 4 °C, and the supernatant was collected. These ADDL preparations were further purified by obtaining the flow-through fraction of 100-kDa molecular mass cutoff filters as described (21).

Human Brain Extracts—The Bioethics Committees and the Biosafety Committees of Mitsubishi Kagaku Institute of Life Sciences, Niigata University, and Kyoto University approved all experiments using human subjects. Freshly frozen brains obtained at autopsy were homogenized to 0.15 g/ml in an ice-cold extraction buffer (either 20 mM Tris-HCl, pH 7.6, 137 mM NaCl, or F12 buffer without L-glutamine and phenol red, containing 1 mM EDTA, 1 mg/ml pepstatin, and complete protease inhibitor mixture (Roche Diagnostics)) using a Potter Teflon/glass homogenizer. Soluble fractions were collected as the supernatant following centrifugation at 104,300 × *g* (TLA100.4) at 4 °C for 1 h. SDS-extractable insoluble fractions were obtained from the pellet by homogenizing in 2% (w/v) SDS and by 1-h gentle shaking at 37 °C, followed by centrifugation for 1 h at 10 °C. Formic acid-extractable fractions were obtained by homogenizing the SDS pellet in 70% formic acid, followed by centrifugation for 1 h. Approximate protein recoveries were 10% for soluble fractions and 90% for insoluble fractions. The possibility of artificial generation of ASPD-like structures from Aβ-(1–42) monomers or of destruction of ASPD-like structures during the extraction procedures was excluded (data not shown). More details are given in the supplemental Experimental Procedures.

***Immunoprecipitations (IP)*—To remove other assemblies (<100 kDa), soluble extracts from AD or NCI brains were concentrated using 100-kDa molecular mass cutoff filters (Millipore). This process was repeated until we obtained AD-derived 100-kDa retentates that contained native ASPDs at ~10–20 μM; this was verified by dot blotting using rpASD1. IPs were performed using an immunocapturing kit 100 MB-IAC Prot G (Bruker Daltonics), according to the manufacturer's instructions, except that 3% (w/v) bovine serum albumin (Sigma A7030) was used to suppress nonspecific binding. Monoclonal ASD antibodies (haASD1 or mASD3) were used for the immunoisolation because of their high affinity for ASPDs. Captured proteins were eluted using Gentle Elution buffer (Pierce),**

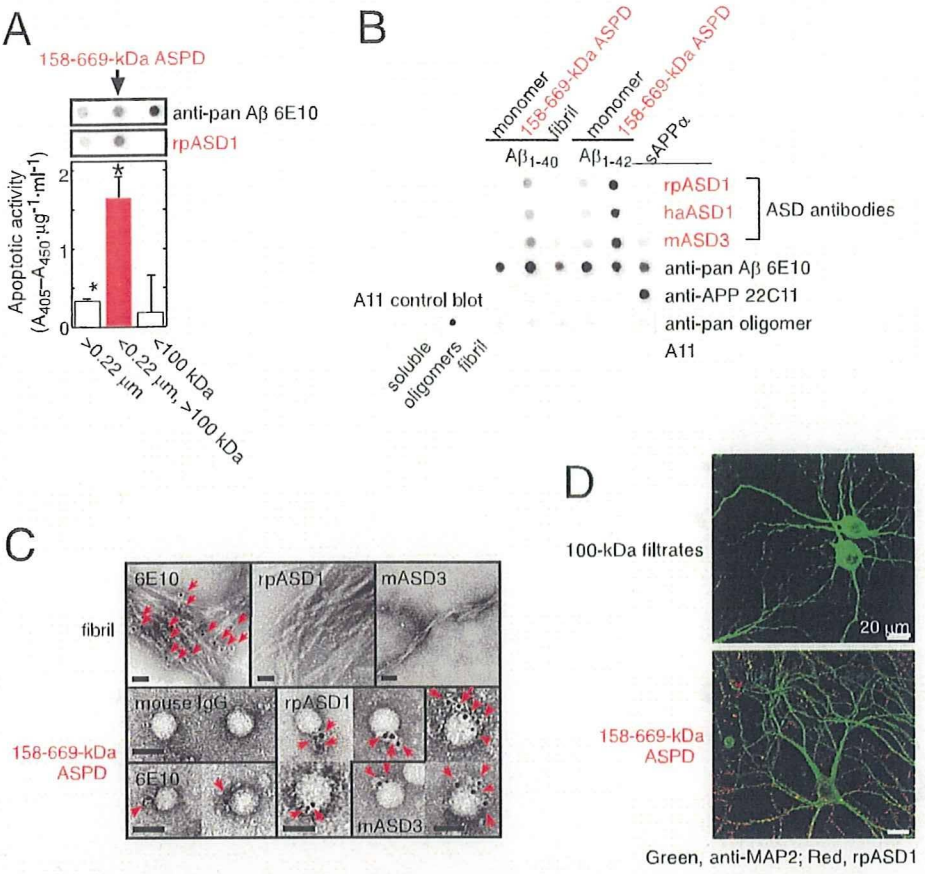

FIGURE 1. **Characterization of ASD antibodies.** *A*, evaluation of two-step filtered fractions (0.22-μm retentates, the 158–669-kDa ASPDs, and 100-kDa filtrates; see Scheme 1 under "Experimental Procedures") by dot blotting using rpASD1 and 6E10 (*upper panel*) and by toxicity assays using rat primary septal cultures (*lower panel*; mean ± S.D.; Games-Howell post hoc test, *, $p < 0.001$, $n = 6$). *B*, dot blotting of Aβ and APP (5 ng/dot). Synthetic ASPDs were prepared *in vitro* either from Aβ-(1–40) or Aβ-(1–42) as described (7). Purified 158–669-kDa ASPD fraction was recovered in 100-kDa retentates as in *A*. Unlike anti-APP-(66–81) (22C11), anti-Aβ-(1–16) (6E10), or A11 antibody, ASD antibodies selectively detected synthetic ASPDs and the 158–669-kDa ASPDs. The control blot membrane for A11 was provided by Invitrogen (supplemental Experimental Procedures). *C*, **immuno-TEM analysis.** ***Arrows*** **show the secondary antibody-conjugated immunogold. 6E10 detected the 158–669-kDa ASPDs weakly, probably because of its low affinity for synthetic ASPDs. rpASD1 and mASD3 showed little reactivity to fibrils but clearly detected the 158–669-kDa ASPDs.** *Bar*, **20 nm.** *D*, **rpASD1 detected intense signals in 27-DIV mature rat hippocampal neurons treated with the 158–669-kDa ASPDs (in *A*) for 30 min but did not detect signals in those treated with the 100-kDa filtrates containing monomers and Aβ-(1–42) assemblies with mass <100 kDa. Z-stack images are shown (supplemental Experimental Procedures).**

because ASPDs retained their structure and toxicity (~100%) after a 60-min exposure to this buffer. The amount of native ASPDs in eluates was immediately examined by dot blotting with polyclonal rpASD1, a suitable antibody for dot blot analysis. Details are given in supplemental Experimental Procedures.

Other Methods—Preparation and screening of ASD antibodies, dot blotting, Western blotting, TEM and immuno-TEM examinations, surface plasmon resonance by Biacore and competitive enzyme-linked immunosorbent assay experiments, pathologic examinations of human brains, *Tg2576* mice experiments, toxicity assays, immunocytochemistry, human neuronal cells, and monkey neural progenitors and neurons, as well as statistics, are described in supplemental Experimental Procedures.

RESULTS

Production and Characterization of ASPD-specific Antibodies—To isolate native ASPDs from AD patients, we raised antibodies against ASPDs in 6 rabbits, 43 mice, and 10 hamsters. As an immunogen, synthetic ASPDs were prepared *in vitro* from 50 μM solutions of Aβ-(1–42) by slowly rotating the solutions for 14 h (38); they included spherical Aβ assemblies of 5–25 nm (>85% of them were 10–15-nm spheres). IgG-class antibodies were purified and named "ASD antibodies," with prefixes indicating the source (rabbit polyclonal as rpASD1; hamster monoclonal as haASD1; mouse monoclonal as mASD3).

We examined the reactivity of ASD antibodies against the most toxic synthetic ASPD fraction separated as follows. Because the mass of the most toxic 10–15-nm ASPDs is almost equal to that of 158-kDa aldolase but does not exceed that of 669-kDa thyroglobulin in sedimentation analysis (38), synthetic ASPDs were further size-separated by means of two-step filtrations (see Scheme 1 under "Experimental Procedures") to concentrate the most toxic 158–669-kDa ASPDs in fraction b, the fraction that passed through 0.22-μm filters but was retained on 100-kDa molecular mass cutoff filters. As expected, 158–669-kDa ASPDs recovered in fraction b included 10–15-nm spheres, as determined by TEM observation (data not shown), and were confirmed to be the most toxic species in toxicity assays (Fig. 1*A*).

Importantly, rpASD1 specifically detected the 158–669-kDa ASPDs in fraction b in dot blotting but had little or no cross-reactivity to fraction a 0.22-μm retentates or fraction c 100-kDa filtrates containing monomers and 5–6-nm particles, which are strongly detected by anti-pan Aβ 6E10 antibody (Fig. 1*A*). We also confirmed that rpASD1 did not cross-react with ADDLs (supplemental Fig. S1*A*). These results indicated that rpASD1 recognizes an epitope that is associated with the most toxic ASPDs but not with ADDLs.

We further characterized rpASD1 and the other ASD antibodies using the most toxic 158–669-kDa ASPDs. As shown in Fig. 1*B*, all ASD antibodies detected primarily the 158–669-kDa ASPDs (prepared from either Aβ-(1–42) or Aβ-(1–40))

TABLE 1

Summary of characters of ASD antibodies and anti-pan Aβ antibodies

The characters of newly established anti-ASPD antibodies (upper three rows) and previously reported anti-pan Aβ antibodies (lower two rows) are summarized. The original epitope mapping data are shown in supplemental Fig. S1*B*; see Fig. 1*A* and supplemental Fig. S3*A* for dot blots and supplemental Table S2 for K_d values determined by Scatchard analysis of enzyme-linked immunosorbent assay data; see Fig. 1*C* (except haASD1) for immuno-TEM and supplemental Fig. S5*A* for toxicity blockade.

Antibody	Preference among Aβ types in dot blotting	K_d for ASPDs	Epitope map	Response to APP in dot blotting	Response to fibrils in immuno-TEM	Blockade of ASPD toxicity
		nM				
rpASD1	ASPD	0.005	Several regions[a]	−	−	+
mASD3	ASPD	0.003	Several regions[a]	±	−	+
haASD1	ASPD	0.0005	Could not be determined[b]	−	−	−
6E10	All types	0.2	Aβ5–9[c]	+	+	−
82E1	All types	ND[d]	Aβ1–5[c]	−	ND	−

[a] The binding of these antibodies to synthetic-ASPDs was most strongly inhibited by N-terminal pentapeptides of Aβ. In addition, the binding was also inhibited by specific sets of non-N-terminal pentapeptides. The data suggest that different Aβ regions exist in close proximity to form the ASPD-specific epitope.
[b] The binding of haASD1 to synthetic-ASPDs was not inhibited by the addition of any pentapeptide, suggesting that haASD1 recognizes a nonlinear epitope formed by noncontiguous Aβ regions.
[c] For 6E10 and 82E1, which did not discriminate ASPDs from other types of Aβ, complete inhibition was attained with a single pentapeptide in each case.
[d] ND means not determined.

but had very low or no cross-reactivity to sAPPα (human secreted form of APP), Aβ monomers, or Aβ fibrils, whereas 6E10 equally detected all these Aβ species and sAPPα (Fig. 1*B*). Consistent with this, ASD antibodies detected 10–15-nm spheres in the 158–669-kDa ASPDs but did not react with fibrils as observed with immuno-TEM under mild fixation conditions (Fig. 1*C*). In accordance with their ASPD preference in dot blots and immuno-TEM, the ASD antibodies showed the highest affinity for the 158–669-kDa ASPDs (K_d 10^{-12}–10^{-13} M; Table 1), rather than for Aβ monomers, fibrils, or sAPPα (supplemental Table S2). These results demonstrated ASPD specificity of all the ASD antibodies. As described above, A11 antibody is a pan-oligomer polyclonal antibody that recognizes epitopes associated with an oligomer state (18, 19, 22). To our surprise, this anti-pan oligomer A11 antibody failed to detect the 158–669-kDa ASPDs (Fig. 1*B*). These results strongly suggested that epitopes recognized by the ASD antibodies are associated with the tertiary structure of ASPDs, which differs from that of A11-positive oligomers, such as Aβ*56 and AβOs, and from that of fibrils. To further elucidate the epitope specificity, we performed epitope mapping by means of competitive enzyme-linked immunosorbent assay using a series of pentapeptides covering the entire Aβ-(1–42) sequence. As summarized in Table 1, no single pentapeptide could compete out binding of the ASD antibodies to the 158–669-kDa ASPDs, suggesting that different Aβ regions exist in close proximity within ASPDs to form ASPD tertiary structure-dependent epitopes that are not present in a single Aβ monomer (supplemental Fig. S1*B*). The ASD antibodies produced only weak or no bands in Western blots under denaturing conditions (data not shown), as would be expected from the fact that they recognize ASPD tertiary structure. We finally examined whether the ASD antibodies are available for detecting ASPDs bound to mature neurons, because we have previously shown that synthetic ASPDs directly induce neuronal cell death, possibly by binding to neuronal cell surfaces (38). As shown in Fig. 1*D*, the ASD antibodies clearly detected synthetic ASPDs bound on mature rat hippocampal neurons (see "Experimental Procedures") when the neurons were briefly treated with the 158–669-kDa ASPDs and fixed under mild conditions, but they did not label neurons treated with the 100-kDa filtrates, which contained monomers and 5–6-nm particles of less than 100 kDa. The characteristics of the antibodies are summarized in Table 1. All of these results demonstrate that the ASD antibodies recognize epitopes that are specific to the surface tertiary structure of ASPDs, which differ from that of ADDLs, A11-positive prefibrillar oligomers, and fibrils.

ASPD-specific Antibody-stained AD Brain—To elucidate whether synthetic ASPD-like assemblies are present *in vivo*, brain sections of patients with clinico-pathologically confirmed AD (41) (n = 10; age 80.4 ± 9.2 years, brain weight 964 ± 82 g, disease duration 10.1 ± 5.5 years) and those of NCI people (n = 7; age 71.3 ± 15.2 years, brain weight 1226 ± 96 g) were immunostained with ASD antibodies. The reactivity of the ASD antibodies in AD patients was strongly associated with brain regions where prominent neurodegeneration had occurred (*e.g.* temporal cortex, frontal cortex, and hippocampus) (Fig. 2*A* and supplemental Fig. S2) but was rarely observed in NCI brains (data not shown). This immunoreactivity in AD brains was associated mainly with plaques and occasionally with neurites and some microvessels and was eliminated by prior treatment of the ASD antibodies with the 158–669-kDa ASPDs (data not shown).

We next compared the reactivity to plaques under various conditions between the ASD antibodies and anti-pan Aβ antibodies, the most widely used antibodies for detecting fibrils in plaques. Although anti-pan Aβ antibodies labeled plaques only in formalin-fixed paraffin sections after pretreatments such as microwaving or formic acid, ASD antibody-specific reactivity was observed most strongly in cryosections and more weakly in formalin-fixed paraffin sections with or without pretreatments (except that haASD1 is available only for cryosections) (Fig. 2*A*). This difference in immunoreactivity to plaques suggested that anti-pan Aβ antibodies and ASD antibodies detect different structures in plaques; anti-pan Aβ antibodies detect fibrils when buried epitopes are exposed by protein-denaturing treatments, whereas ASD antibodies are considered to detect tertiary structure-dependent epitopes on putative human ASPD counterparts under conditions where the native structure of proteins is preserved. To confirm this, we performed biochemical fractionation of AD brains and examined whether these antibodies reacted with insoluble or soluble fractions. Consistent with previous data that fibrils include an insoluble core of plaques (42), anti-pan Aβ antibodies reacted mainly (>85%)